NASA CONTRACTOR REPORT

NASA CR-2650

STRUCTURE OF ATMOSPHERIC TURBULENCE IN THE FRICTION LAYER BELOW 500 METERS

Stephen J. Maas and James R. Scoggins

Prepared by
TEXAS A&M UNIVERSITY
College Station, Texas
for George C. Marshall Space Flight Center

NATIONAL AERONAUTICS AND SPACE ADMINISTRATION • WASHINGTON, D. C. • FEBRUARY 1976

1. REPORT NO.	2. GOVERNMENT ACCESSION NO.	3. RECIPIENT'S CATALOG NO.
NASA CR-2650		

4. TITLE AND SUBTITLE	5. REPORT DATE
Structure of Atmospheric Turbulence in the Friction Layer Below 500 Meters	February 1976
	6. PERFORMING ORGANIZATION CODE M165

7. AUTHOR(S)	8. PERFORMING ORGANIZATION REPORT #
Stephen J. Maas and James R. Scoggins	

9. PERFORMING ORGANIZATION NAME AND ADDRESS	10. WORK UNIT NO.
Center for Applied Geosciences Texas A&M University College Station, Texas	11. CONTRACT OR GRANT NO. NAS8-29764
	13. TYPE OF REPORT & PERIOD COVERED Contractor Report

12. SPONSORING AGENCY NAME AND ADDRESS	14. SPONSORING AGENCY CODE
National Aeronautics and Space Administration Washington, D. C. 20546	

15. SUPPLEMENTARY NOTES

Prepared under the technical monitorship of the Aerospace Environment Division, Space Sciences Laboratory, NASA-Marshall Space Flight Center.

16. ABSTRACT

Data consisting of measurements of wind direction and speed, vertical velocity, and temperature from several levels on the 444-m tower near Oklahoma City instrumented by the National Severe Storms Laboratory were analyzed to determine the nature of turbulence in the lowest 500 m of the friction layer. Turbulence quantities were calculated from the covariances between observed variables over periods ranging from 5 min to 1 hr. It was found that in some cases parameters such as mean wind speed, shearing stress, and vertical heat flux could be expressed by simple equations for periods of 15 min to 1 hr. Changes in these quantities with time are related to changes in vertical motion and stability.

Power spectra were calculated for sequential 15-min, 30-min, and 1-hr periods for several levels on the tower. The effects of stability, wind speed, and surface roughness on the spectra of longitudinal and lateral velocity are examined, along with the effect of height on the spectrum of vertical velocity. The existence of an inertial subrange in the spectra of the horizontal velocity components also is evidenced.

The region penetrated by the tower is shown to be composed of a lower region in which mechanical turbulence dominates and an upper region dominated by convective turbulence.

17. KEY WORDS	18. DISTRIBUTION STATEMENT
Boundary layer, turbulence, wind shear, atmospheric stability, friction velocity, surface roughness	Category 47

19. SECURITY CLASSIF. (of this report)	20. SECURITY CLASSIF. (of this page)	21. NO. OF PAGES	22. PRICE
Unclassified	Unclassified	76	$4.75

For sale by the National Technical Information Service, Springfield, Virginia 22161

FOREWORD

The research reported in this document was motivated by the need for a definition of low level wind shear and turbulence environments for the design and evaluation of aeronautical and aerospace systems. The objectives of this research are to investigate the structure of atmospheric turbulence in the region of the lower atmosphere including and extending above the surface boundary layer into the region where stress and vertical heat flux may not be considered constant, and to establish interrelationships between turbulence parameters for the region of the atmospheric boundary layer below a height of approximately 500 m. This research was conducted by the Texas A&M University for the National Aeronautics and Space Administration, George C. Marshall Space Flight Center, Huntsville, Alabama, under the direction of Dr. George H. Fichtl of the Aerospace Environment Division. The support for this research was provided by Mr. John Enders of the Aviation Safety Technology Branch, Office of Advanced Research and Technology, NASA Headquarters.

TABLE OF CONTENTS

LIST OF TABLES

LIST OF FIGURES

LIST OF FIGURES (Continued)

LIST OF FIGURES (Continued)

LIST OF FIGURES (Continued)

1. INTRODUCTION

The objectives of this research are to investigate the structure of atmospheric turbulence in the region of the lower atmosphere including and extending above the surface boundary layer into the region where stress and vertical heat flux may not be considered constant, and to establish interrelationships between turbulence parameters for the region of the friction layer below a height of approximately 500 m. Most previous studies of turbulence in the boundary layer are for heights below about 150 m.

The determination of the turbulent nature of the flow below about 500 m was facilitated by the fact that shearing stresses and vertical heat flux could be calculated directly from wind speed and direction, vertical velocity, and temperature fluctuations measured on a tower 444 m high. This eliminated the need to calculate shearing stresses from the wind profiles, a method that relies on the assumption that the stress is proportional to the mean wind shear, and indeed allowed a test of the hypothesis of the momentum exchange coefficient to be made. Similarly, because fluctuations of both temperature and vertical velocity were measured at the same levels, it was not necessary to rely on the lapse rate of temperature in calculating vertical heat flux. Therefore, the first-hand nature of this research strengthens the validity of the findings presented herein.

The style of this manuscript follows the format of Boundary-Layer Meteorology.

2. BACKGROUND TO PRESENT RESEARCH

The friction layer has been described as that portion of the lower atmosphere adjacent to the ground in which turbulent stresses are significant (Lettau, 1950). In this layer, which may extend to a height of around 1 km, the shearing stress and vertical heat flux are known to vary with height, but in the lowest layer in which the stress and heat flux are observed to vary less than 20 per cent is called the surface boundary layer, and generally extends to a height of from 20 to 200 m above the ground (Lumley and Panofsky, 1964). Tennekes (1973) states that the upper limit of the height of the boundary layer is about 100 m, which is within the above limits. The remainder of the friction layer above the surface boundary layer and extending to where the fluid motion approximates geostrophic flow is often called the Ekman layer, due to the change of wind speed and direction with height observed by Ekman in this region of the atmosphere (Sutton, 1953).

The turbulent nature of the surface boundary layer has drawn the attention of numerous investigators; consequently, most of the turbulent processes in this layer are adequately understood. Because the bulk of the findings has been derived from studies involving instrumented towers of the heights of 150 m or less, the variation of turbulence parameters in the remainder of the friction layer is still poorly understood. Some investigations of the upper region have been carried out using balloon observations, such as the study of the trade wind structure by Charnock, Francis, and Sheppard (1956), but the volume and quality of information must be considered below that obtainable from instrumented towers. This is due in part to the balloon's inability to react to small-scale turbulent fluctuations, and also due to the fact that turbulence parameters must be calculated from mean wind profiles. A few studies have been made using very tall towers, notably one by Thuillier and Lappe (1964) involving observations from a 433-m tower near Dallas, Texas.

In the study of the turbulent character of the friction layer, two terns that are very useful and can be calculated directly from instrumented tower data are the covariances involving the fluctuations in component wind speed and temperature, viz., $\overline{u_i'(t)\ u_j'(t)}$ and $\overline{\theta(t)\ u_j'(t)}$, in which $u_i'(t)$ and $u_j'(t)$ are the instantaneous deviations from the average component wind speeds, and $\theta(t)$ is the instantaneous deviation from the average temperature, defined by the equations,

$$u_i(t) = \overline{u}_i + u_i'(t) \ , \tag{1}$$

$$u_j(t) = \overline{u}_j + u_j'(t) \ , \tag{2}$$

and

$$T(t) = \overline{T} + \theta(t) \ . \tag{3}$$

The quantities on the left-hand side are instantaneous observed values and the overbar indicates the average of the quantity over the sampling period. The subscripts i and j may take the values 1, 2, or 3 and correspond to the longitudinal (u), lateral (v), and vertical (w) wind components, respectively.

The tensor involving velocity fluctuations, when multiplied by the average air density, $\overline{\rho}$, becomes a force due to the transport of momentum by the turbulence. Those forces are referred to as Reynolds stresses, or, when the i and j components are chosen to be orthogonal, shearing stresses. Utilizing all the possible combinations of u_i' and u_j' gives a total of nine terms, but in practice the stresses involving the product of the longitudinal or lateral and the vertical component velocities are most useful in that they describe the upward or downward transport of horizontal momentum. These shearing stresses are defined by the equations,

$$\tau_{xz} = -\overline{\rho}\ \overline{u'w'} \ , \tag{4}$$

and

$$\tau_{yz} = -\overline{\rho}\ \overline{u'w'} \ . \tag{5}$$

When the $\theta u_j'$ term is multiplied by $C_p\overline{\rho}$, where C_p is the specific heat of air at constant pressure, the result represents the heat transported by turbulent fluctuations. Generally the vertical turbulent transport of heat is most important, and is defined by

$$H = C_p\overline{\rho}\ \overline{\theta w'} \ . \tag{6}$$

Studies of the variation of shearing stresses with height from

balloon observations (in a right-handed coordinate system with the longitudinal axis parallel to the surface mean wind direction) indicate that τ_{xz} decreases with height from a positive maximum value at the surface, and becomes negative in the upper region of the friction layer; τ_{yz} decreases from zero at the surface to a minimum at around 200 to 300 m above the surface, and then again approaches zero near the top of the friction layer (Charnock et al., 1956; Bradham, 1970). Studies such as that by Campbell, Hansen, and Dise (1970) that employed stresses calculated from covariances demonstrate that the detailed change of observed stress values with height in the layer penetrated by instrumented towers is more variable than indicated by studies that employed balloon observations, with both increases and decreases in each of τ_{xz} and τ_{yz} reported. Few direct observations of vertical heat flux have been made and generally the variation of heat flux with height is inferred from temperature profiles, but the study by Campbell et al. cited above indicates that at least in the lowest 32 m of the friction layer the vertical heat flux is roughly constant or increases with height during the early afternoon when surface heating should be at a maximum.

The shearing stress at the surface normally is not measured but can be obtained (Lumley and Panofsky, 1964) from the wind speed observed near the ground by solving the familiar logarithmic wind profile equation,

$$\bar{V} = \frac{u_*}{k} \ln\left(\frac{z}{z_o}\right) , \tag{7}$$

for the surface friction velocity u*. In the equation $\bar{V}$ is the observed average wind speed, z the height, z_o the roughness length, and k the von Karman constant with a numerical value of approximately 0.4. The surface shearing stress, τ_o, is then given by

$$\tau_o = \bar{\rho} u_*^2 , \tag{8}$$

in which $\bar{\rho}$ is the mean air density proximal to the ground. Although the derivation of the logarithmic equation, or "log law," assumes neutral (adiabatic lapse rate) conditions, its validity has been verified for any stability condition in the very shallow layer adjacent to the ground. Lumley and Panofsky have explained this fact

as due to the dominance of the production of mechanical turbulent energy (by wind shear) over the production of buoyant turbulent energy (by convection) next to the ground. These authors note that over rough terrain in strong wind conditions the log law may be valid up to 5 m or more even when the vertical heat flux is large. While average wind profiles usually may obey the log law only in the first few meters, there is evidence that under near-neutral conditions mean wind profiles over periods equal to or greater than around 10 min may be logarithmic to a height of 150 m, or roughly 10 per cent of the friction layer (Thuillier and Lappe, 1964; Carl, Tarbell, and Panofsky, 1973; H. Tennekes, 1973). The variation of vertical velocity with height is largely dependent upon stability and the mesoscale development of convection. It is often possible to detect a regular periodic nature in the field of upward and downward motion passing over a location, as was demonstrated by Kjelaas, et al. (1974) using an array of acoustic sounders and microbarographs.

Mean wind profiles are assumed to be related to the shearing stresses through the application of the closure hypothesis of the momentum exchange coefficient, that states that downward flux of momentum is proportional to the vertical shear of the mean wind (Lumley and Panofsky, 1964). Accordingly, the stresses may be defined by

$$\tau_{xz} = \overline{\rho} K_{xz} \frac{\partial \overline{u}}{\partial z} \tag{9}$$

and

$$\tau_{yz} = \overline{\rho} K_{yz} \frac{\partial \overline{v}}{\partial z} , \tag{10}$$

where τ_{xz} and τ_{yz} are the shearing stresses as before, $\overline{\rho}$ the average air density, $\partial\overline{u}/\partial z$ and $\partial\overline{v}/\partial z$ the shears of the mean component wind velocities, and K_{xz} and K_{yz} the coefficients of eddy viscosity corresponding to τ_{xy} and τ_{yz}, respectively. Balloon observations in the lower atmosphere indicate that K_{xz} increases with height in the lower region of the friction layer to a maximum at around 300 m, then decreases to a minimum at around 700 m, and finally increases again with height near the top of the friction layer; K_{yz} was found generally to decrease with height through the friction layer (Charnock

et al., 1956; Bradham, 1970). For a logarithmic wind profile the eddy viscosity is proportional to height, which is in agreement with the observed increase in K_{xz} in the lower part of the friction layer.

While the shearing stresses and vertical heat flux are important in explaining the general turbulent transfer in the friction layer, the nature of the turbulent eddies themselves in the transfer process can be examined best by spectral analysis. Power spectra of the u, v, and w components indicate the relative importance of harmonics to the turbulent oscillations. Lumley and Panofsky (1964) state that for small-scale oscillations the contributions to the total variance is the same for all components, but as the scales increase a marked anisotropy appears in the spectra, with the vertical component becoming systematically different from the horizontal components. The smaller scales are due to mechanical turbulence, while the larger scales are influenced primarily by convection and mesoscale activity. Large vertical components at low frequencies are possible only during strong convection, and oscillations on the order of 2 min in both the vertical and lateral components are strongly influenced by stability (Lumley and Panofsky). The other important feature of power spectra is the existence of an inertial subrange in the group of small-scale eddies in which the kinetic energy is partitioned in proportion to $K^{-5/3}$, where K is the wave number (Sutton, 1953). Lumley and Panofsky report that the existence of this feature is verified fairly well by numerous turbulence studies.

3. INSTRUMENTATION AND DATA

A. Source, Amount, and Types of Data

Three sets of data, consisting of detailed wind and temperature measurements collected from the 444-m meteorological tower facility of the National Severe Storms Laboratory (NSSL) located 6 mi north of Oklahoma City, were used in this investigation. The characteristics of the data sets are summarized in Table I. Temperature values were reported to the nearest hundredth of a Celsius degree, wind speed to the nearest tenth of a m sec^{-1}, wind direction to the nearest tenth of a degree of azimuth, and vertical velocity to the nearest hundredth of a m sec^{-1} for Sets I and II; the accuracy of measurements in Sets I and II was one order of magnitude better than in Set III.

The data were provided by the National Severe Storms Laboratory (NSSL) of the National Oceanic and Atmospheric Administration (NOAA), Norman, Oklahoma. The sets were received in the form of magnetic tapes but were transferred subsequently to magnetic discs to simplify their use in computational procedures. Although Sets I and II are a few seconds short of being multiples of an exact hour in length, statistical operations involving this shortage will be referred to as being from a complete 1-hr period. In other words, the average wind speed over the entire set of observations in Set I will be referred to as the "hour mean wind speed."

B. Types of Instrumentation Used

The instrumentation of the 444-m NSSL tower facility has been described in detail by Carter (1970).

Measurements of horizontal wind speed and direction at all levels were made by using Bendix Model 120 Aerovanes. Each instrument is mounted 3.04 m (10 ft) from the tower on a boom aligned to an azimuth angle of 240 deg. The effect of the tower on measured wind speeds is considerable only for wind directions between 350 and 70 deg; the prevailing wind direction during this study was around 170 deg. The sensor has a speed threshhold of 0.84 m sec^{-1}, an accuracy of $\pm$0.25 m sec^{-1}, and a distance constant (defined as the

TABLE I

Summary of the three data sets obtained from the NSSL meteorologically-instrumented tower facility

DATA SET	DATE	TIMES (CST) START/STOP	OBSERVATIONS	Δt (SEC)	INSTRUMENTED LEVELS (m) SPEED & DIR.	TEMP.	VERT. MOTION
I	18 June 1971	13:35:04/ 14:34:48	1793	2	26,45,90, 177,266,355, 444	26,45,90, 177,266,355, 444	26,177,444
II	4 May 1972	12:00:00/ 15:59:50	1439	10	26,45,90, 177,266,355, 444	26,45,90, 177,266,355, 444	26,177,444
III	11 June 1973	08:00:02/ 11:00:02	10800	1	89,266,444	89,266,444	89,266,444

"wind passage by the propellor required for the anemometer output to reach 63 per cent of a step speed change") of 4.66 m. Carter (1970) concludes from the instrument response criteria that estimates of gust amplitudes of higher frequency speed and direction improve with increasing mean wind speeds, so that measurements of finer scale frequency are more accurate near the top of the tower than near the ground.

The sensitivity of turbulence measurements made by using the Model 120 Aerovane has been described by Scoggins (1966), who compared the output of several wind sensors simultaneously exposed to the same wind conditions. The response of the Aerovane as compared to three other anemometers (generally considered "more sensitive" to turbulent fluctuations) at wind speeds comparable to those observed in the data set is shown in Table II. Of the four instruments studied, the Aerovane recorded both the lowest mean wind speed and variance values over the sampling period; however, the portion of the total variance not measured is due almost exclusively to fluctuations with periods shorter than 5 sec.

Due to considerations concerning the calculation of power spectra, the shortest period of interest in this report is 4 sec. The power spectra in Fig. 1 show the observed partitioning of the total variance among the various harmonics for each instrument; the solid vertical line denotes a harmonic period of 4 sec on the abscissa. The portion of the figure to the left of the vertical line, which includes the range of fluctuations considered in this paper, shows that the spectral curve associated with the Aerovane approximates those obtained from the other (more sensitive) anemometers. Only to the right of the vertical line does the variance attributed to the various harmonics of the Aerovane differ markedly from the other wind instruments. Thus, for the range of frequencies under investigation in this report, the Model 120 Aerovane appears to be adequate.

The temperature sensors installed at each level were Yellow Springs Instruments resistance thermistors mounted on heat sink stainless steel probes, which were housed in Climet Model 016-1

TABLE II

Comparative response of various wind-measuring instruments

ANEMOMETERS	MEAN WIND SPEED (m sec^{-1})	VARIANCE ABOUT MEAN (m^2 sec^{-2})	PERCENT VARIANCE FOR P>5 sec
B&W 50	6.73	1.66	0.89
CLIMET C1-14	7.77	1.14	0.91
B&W 101	7.97	2.26	0.93
AEROVANE 120	6.16	0.99	0.99

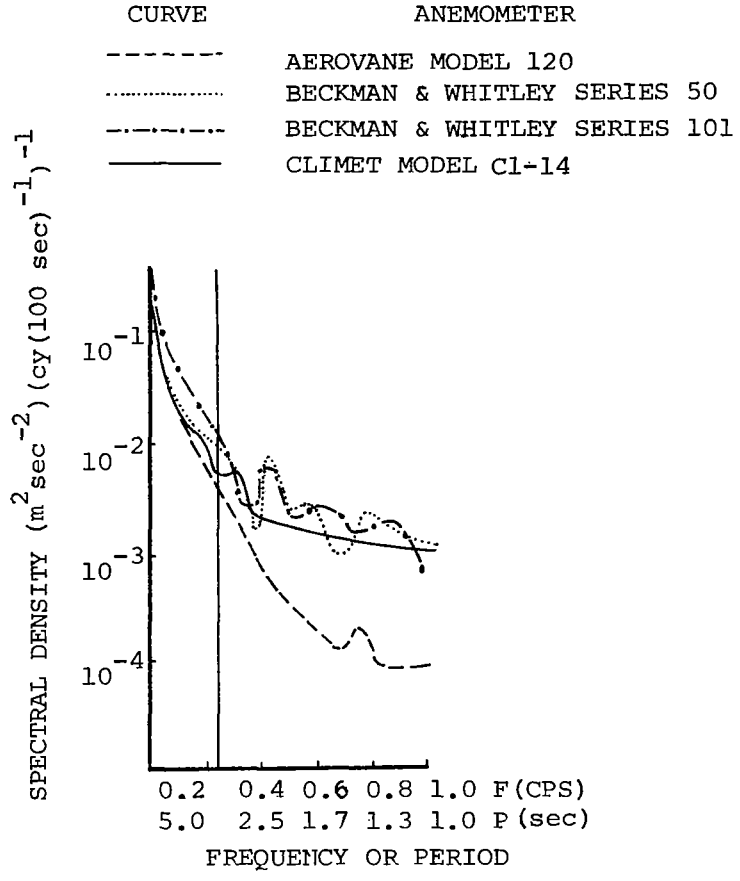

Fig. 1. Power spectra obtained from various wind-measuring instruments.

motor-aspirated radiation shields. These were affixed on the underside of the boom exposing the wind instruments. The thermistors have a temperature range of -30 C to +50 C, a linearity deviation of $\pm$0.05 deg C, and a time response (time to indicate 63 per cent of a step temperature change) of $\leq$0.25 sec.

Instrumentation to record vertical velocity consisted of R. M. Young Company Model 1200 anemometers with polyethylene propellers. No response specifications for this instrument were obtained, but the response of the Model 1200 anemometer is known to be at least as good as that of the Aerovane.

C. Synoptic Conditions

The dominant synoptic feature on the day Data Set I was obtained (18 June 1971) was a frontal system stretching from the Great Lakes across the northern Great Plains to a weak cyclone in western Kansas. Although the front triggered squall-line activity throughout the day in Iowa and southern Minnesota, the front remained stationary some 400 mi to the northwest of the NSSL tower site.

At 0600 CST (1200 GMT) skies over central Oklahoma were clear and temperatures ranged a few degrees above 70 F. Winds were from the south to southwest at around 5 m sec^{-1}. By 1200 CST (1800 GMT) the temperature had climbed to above 90 F and a few towering cumuli had begun to appear. The frontal system was in the process of dissipating and winds had become steady from the southwest at around 7 m sec^{-1}. A few scattered thunderstorms had developed in northeastern Arkansas. By 1500 CST (2100 GMT) the front had dissipated and the associated cyclone was filling -- winds around the NSSL site had switched direction more toward the south and southeast and had decreased in speed to between 5 and 7 m sec^{-1}. Temperatures remained around 95 F and the sky had become partly cloudy with cumuli and towering cumuli having bases in the range from 5000 to 7500 ft predominating. None of the radar summaries for the day showed shower activity in Oklahoma.

The combination of strong insolation, warm air temperature, and the gently rolling terrain would tend to favor convection at the tower

site during the sampling period. The absence of sufficient water vapor (dew-point depressions were in excess of 20 F throughout the day), presumably due to the southwesterly air flow, tends to explain the absence of marked convective cloud development as evidenced by the scarcity of clouds. The local turbulence should not have been solely convective in nature, however, due to the steady moderate winds which should have led to a thorough mixing of the air near the surface. Therefore, the most likely causative conditions for turbulence existing during the sampling period on 18 June 1971 should have been both mechanical and convective.

The major synoptic influence on the local weather conditions during the time period covered by Data Set II was provided by an extensive anticyclonic system covering the greater part of the central United States. Although the center of the system remained stationary in southern Arkansas, the pressure gradients on the back side of the anticyclone were observed to strengthen during the period. Some organized cloud regions existed to the north in Nebraska and Missouri, but no significant weather was indicated at the tower site throughout the sampling period. Temperatures were in the low 70's through the early afternoon, with south-easterly surface winds increasing from around 10 to 20 m sec^{-1} through the period.

The major synoptic feature during the time period covered by Data Set III was a stationary front extending from the Great Lakes to a weak low-pressure area in Colorado. The general circulation at the surface was that of the warm, moist influx from the Gulf of Mexico common in June. Conditions at the tower site remained generally the same for the 3-hr period, with temperatures in the upper 60's and 10-15 m sec^{-1} winds sweeping in from the south. Skies in the Oklahoma area ranged from partly cloudy to overcast with cumulus humilis the predominant cloud type reported. There was some thunderstorm activity to the south in Texas but none reported north of the Red River during the recording period.

4. ANALYSIS OF DATA

A. Prewhitening of Data

An examination of wind observations contained in the three data sets revealed an obvious long-term trend in data Set II and also some indication of trend in Set III. Mean values of scalar wind speed over sequential 5-min periods at the 26-m level from Set II are shown in Fig. 2, along with interpolated values of geostrophic wind speed over that period. The interpolation was obtained from values of the surface pressure gradients taken from synoptic charts at the beginning and end of the time period in Fig. 2. Apparently the roughly linear trend in the observed wind-speed values is due to the increase with time in the pressure gradient, as evidenced by the slope of the line representing the geostrophic wind speeds.

A filter function was designed to remove the effects of the trend in calculations of turbulence quantities and spectra. The filter is symmetrically-weighted and is of the form

$$R(f) = w_o + 2\sum_{k=1}^{n} w_k \cos(2k\pi f \Delta t) \; ; \; n=6 \; , \qquad (11)$$

where w_k are the weights, f is frequency, and Δt is the time interval between observations to which the weights are applied. The values of the 13 weights are given in Table 3.

TABLE III

Values of the filter weights, w_k

k	w_k
0	0.22383
1	0.10700
2	0.09348
3	0.07465
4	0.05448
5	0.03634
6	0.02215

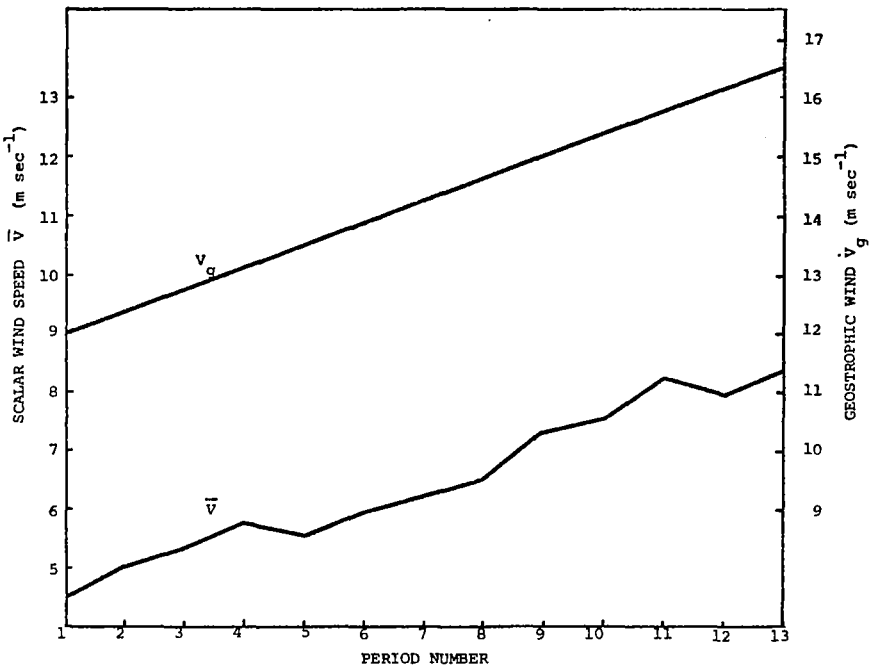

Fig. 2. Comparison of the variation with time of scalar wind speed and computed geostrophic wind speed V_g for Data Set II. Period number refers to sequential 5-min periods over which the mean scalar wind speed, $\bar{V}$, at the 26-m level was calculated.

The filter response as a function of frequency is shown in Fig. 3, with Δt chosen to be 30 sec. It can be seen that harmonics with periods less than about 5 min would be negligibly affected by the prewhitening process; however, over 90 per cent of the variability due to harmonics with periods of around 20 min or greater would be eliminated. In the determination of spectra from prewhitened data, the true spectrum can be recovered from the calculated spectrum by use of the relation:

$$\Phi(f)_{true} = \frac{\Phi(f)_{computed}}{(1-R(f))^2} \qquad (12)$$

where $\Phi(f)_{true}$ and $\Phi(f)_{computed}$ are the true and calculated spectra, respectively, and R(f) is the filter function.

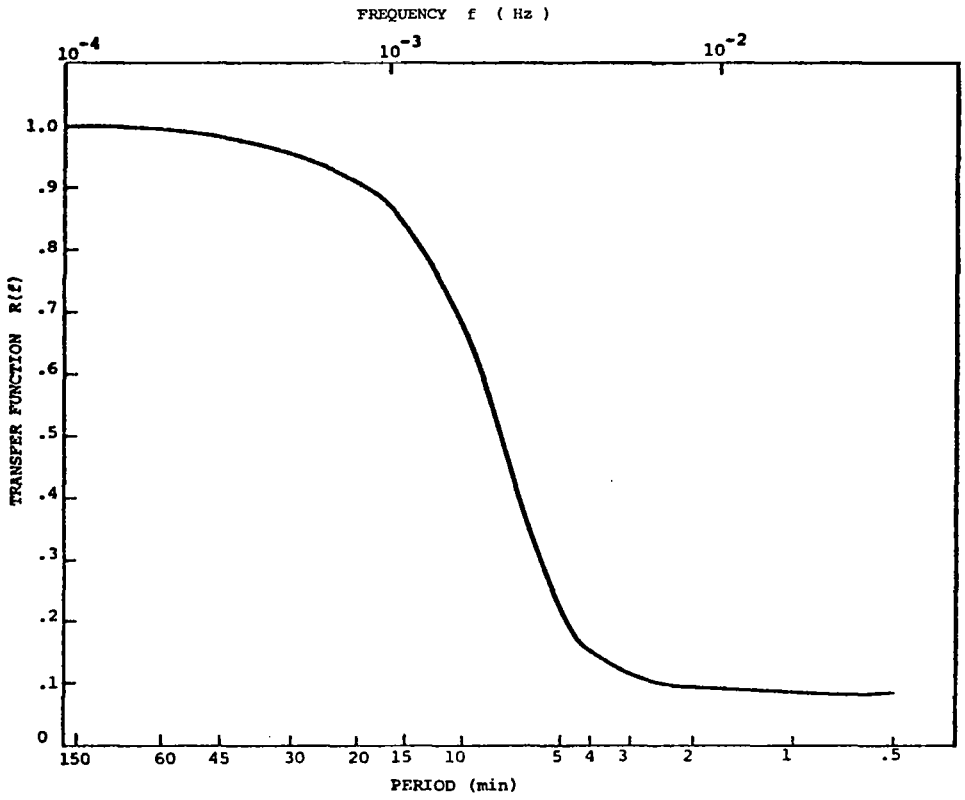

Fig. 3. Filter function used in the computation of turbulence quantities and spectra to remove the effects of trend in Data Sets II and III.

B. Vertical Motion and Fluxes of Momentum and Heat

Average profiles of vertical velocity, $\bar{w}$, over the 1-hr and sequential 15-min periods for data Set I are shown in Fig. 4. Upward motion dominates the lower two-thirds of the tower height for the hour mean profile, but the 15-min mean profiles show a high degree of variability. This variability is better illustrated in Fig. 5, which displays 5-min average values of vertical motion versus time and height from Set I in the manner of a cross section. The temporal distributions cannot be translated strictly into spatial distributions by application of Taylor's hypothesis because of the distorting effect of the vertical shear of the advecting wind on the larger eddies. Powell and Elderkin (1974) have shown that Taylor's hypothesis holds quite well provided that the frequency, n, of the turbulent oscillations complies with the criteron

$$\frac{2\pi n}{\left(\frac{d\bar{u}}{dz}\right)} \geq 3.6 , \qquad (13)$$

where $d\bar{u}/dz$ is the shear of the mean advective wind velocity. A typical value of the vertical shear of mean longitudinal wind speed (assumed representative of the advective velocity) near the ground for this study is 0.1 sec^{-1}, so that n by (13) must be greater than or equal to about 3.6 cycles min^{-1}, clearly representing eddies too small to survive the averaging process. However, the largest structures, bordering on the mesoscale, probably do remain spatially intact to a fair degree in the form shown in Fig. 5 because their great size can be affected only partially by shear during the recording period. This scale is certainly larger than the largest individual eddies themselves, but of a scale so as to show the contribution of eddies to the almost-mesoscale structure which determines the mean wind profiles. Thus, Fig. 5 illustrates the general large-scale field of vertical motion.

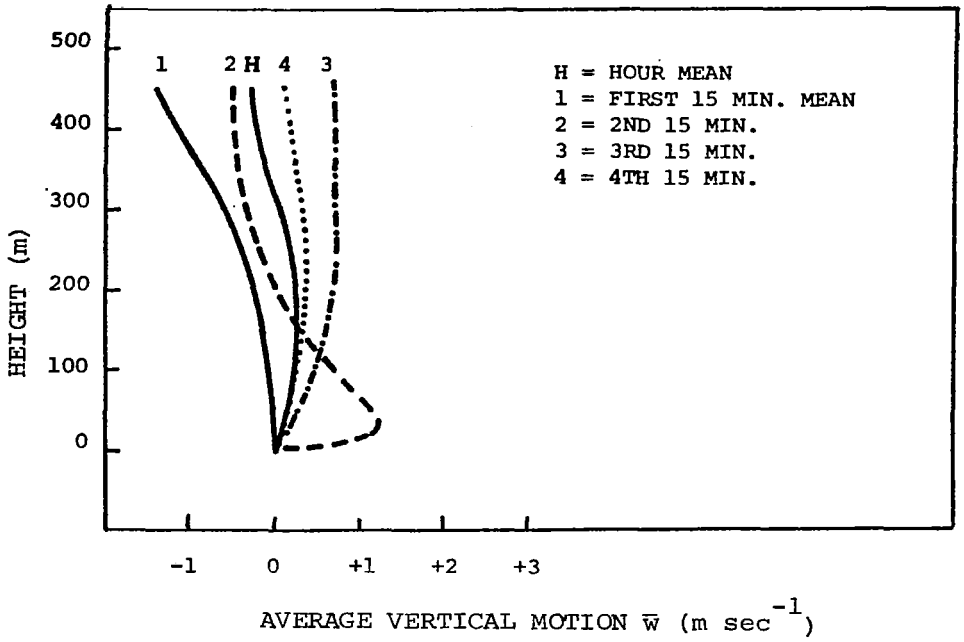

Fig. 4. Average vertical velocity for the 15-min and 1-hr periods for Data Set I.

The structure shown in Fig. 5 indicates that an organized system of vertical motion was in existence during the hour. Examination reveals:

(1) In the cross section, the time span of positive w is noticeably larger than that of negative w;

(2) The organization of successive upward and downward maxima is most noticeable above around 150 m;

(3) There is a general increase with height of $|w|$;

(4) The maximum mean downward velocities are 2.5 times greater than the maximum mean upward velocities; and

(5) Each upward- or downward-motion segment contains a pair of maxima, with one being larger or more intense than the other.

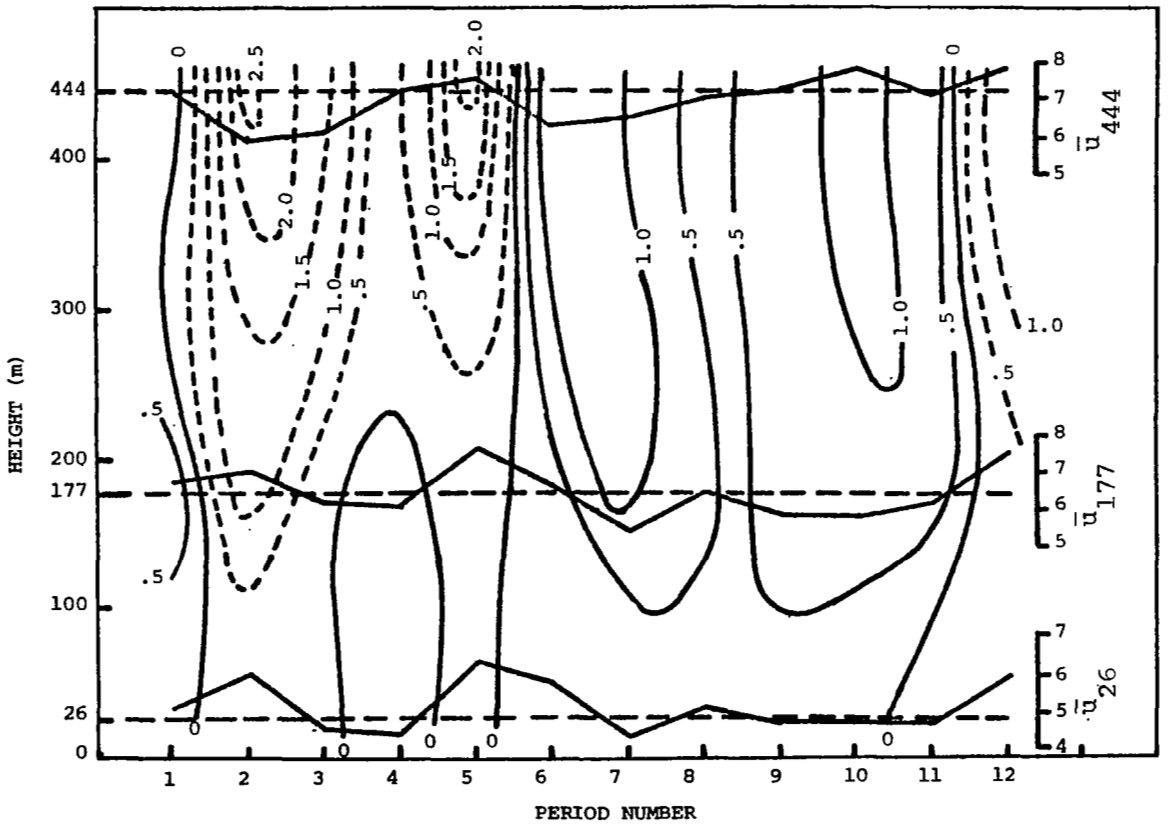

Fig. 5. Mean vertical velocity as a function of time and height for Data Set I. Period number refers to sequential 5-min periods over which averages were determined. Solid lines indicate upward motion, dashed lines downward motion, in m sec^{-1}. Traces of 5-min mean longitudinal velocity, $\bar{u}$, in m sec^{-1} at three heights are superimposed.

The explanation of some of these characteristics lies in the actual physical nature of the large-scale systems and will be discussed in Section 5. Two possible explanations for the lack of organization in the w field below 150 m are:

(1) The mechanical turbulence due to wind shear near the surface disrupts the large-scale structures in the manner described in the previous paragraph. This would presuppose that if the large-scale structures are not produced by local turbulent activity, they can survive in spite of the turbulence near the ground.

(2) Scorer and Ludlam (1953) theorized that small eddies rising from near the surface become aggregated into larger, more organized eddies with height. Thus, the random contributions to vertical motion by many small eddies would not lead to organized fluctuations near the surface, but once a number of these eddies contribute their buoyancy to make a larger system the resulting motion becomes observable. This explanation allows the large-scale features to be the result of local turbulent transfer.

It is likely that both processes contribute to some degree to the observed effect.

Average profiles of vertical velocity for Data Sets II and III are shown in Fig. 6. Averaging periods of 1 hr were used in the analysis of Set II, while 30-min periods were used for Set III. The two sets of profiles in Fig. 6 are similar and differ from the results presented in Fig. 4 in that the motion is upward throughout the whole tower height for almost every profile (a small region of downward motion is indicated in the third profile from Set III). This is conceivably due to the presence of a less-developed convective regime at the times Sets II and III were taken--downwellings of cooler air become organized only after the convective activity has been sustained for some time (Scorer and Ludlam, 1953).

The development of convective activity can be traced in Fig. 7, which displays 5-min average values of vertical velocity from Set III in the same manner as in Fig. 5 (the upper part of Fig. 7 will be discussed later). During approximately the first half of the 3-hr period, upward and downward motions are relatively weak and poorly

organized; after around 0930 CST, maxima and minima begin to extend through the entire depth of the layer penetrated by the tower, and absolute values of vertical velocity exceed 1 m sec^{-1}. In the last hour of the data set, upward and downward motions are well organized and appear to be taking on a periodic nature, though not to the degree exhibited in Fig. 5.

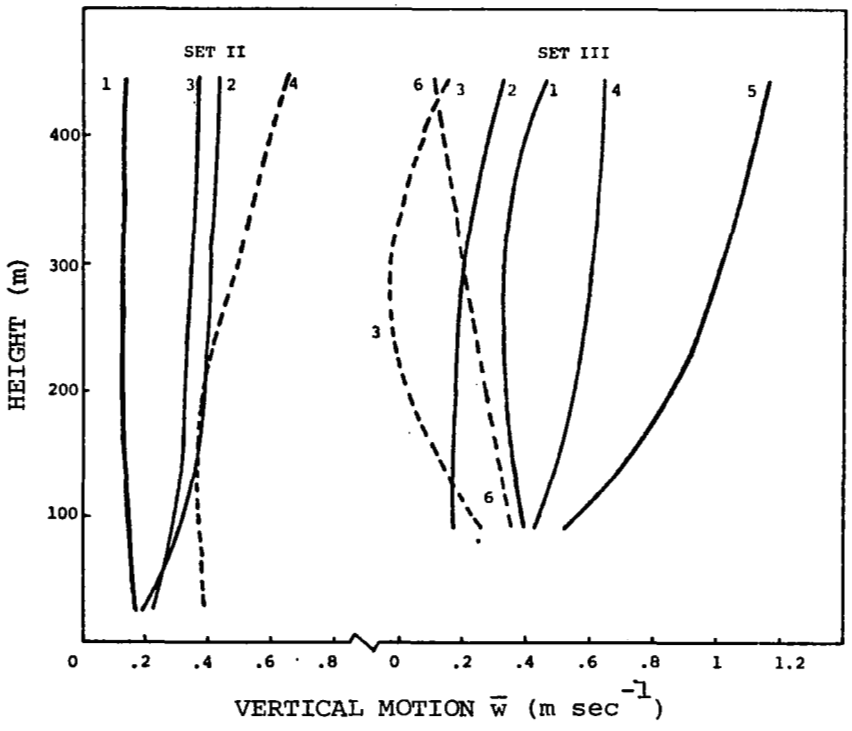

Fig. 6. Sequential average profiles of vertical velocity for Data Sets II and III. The averaging period was 1 hr for Set II and 30 min for Set III. Profile numbers refer to sequential averaging periods.

The variation with height of the component shearing stresses for Set I is shown in Fig. 8. Values of τ_{xz} and τ_{yz} above the surface were calculated by using (4) and (5), respectively; because the longitudinal axis was chosen parallel to the surface

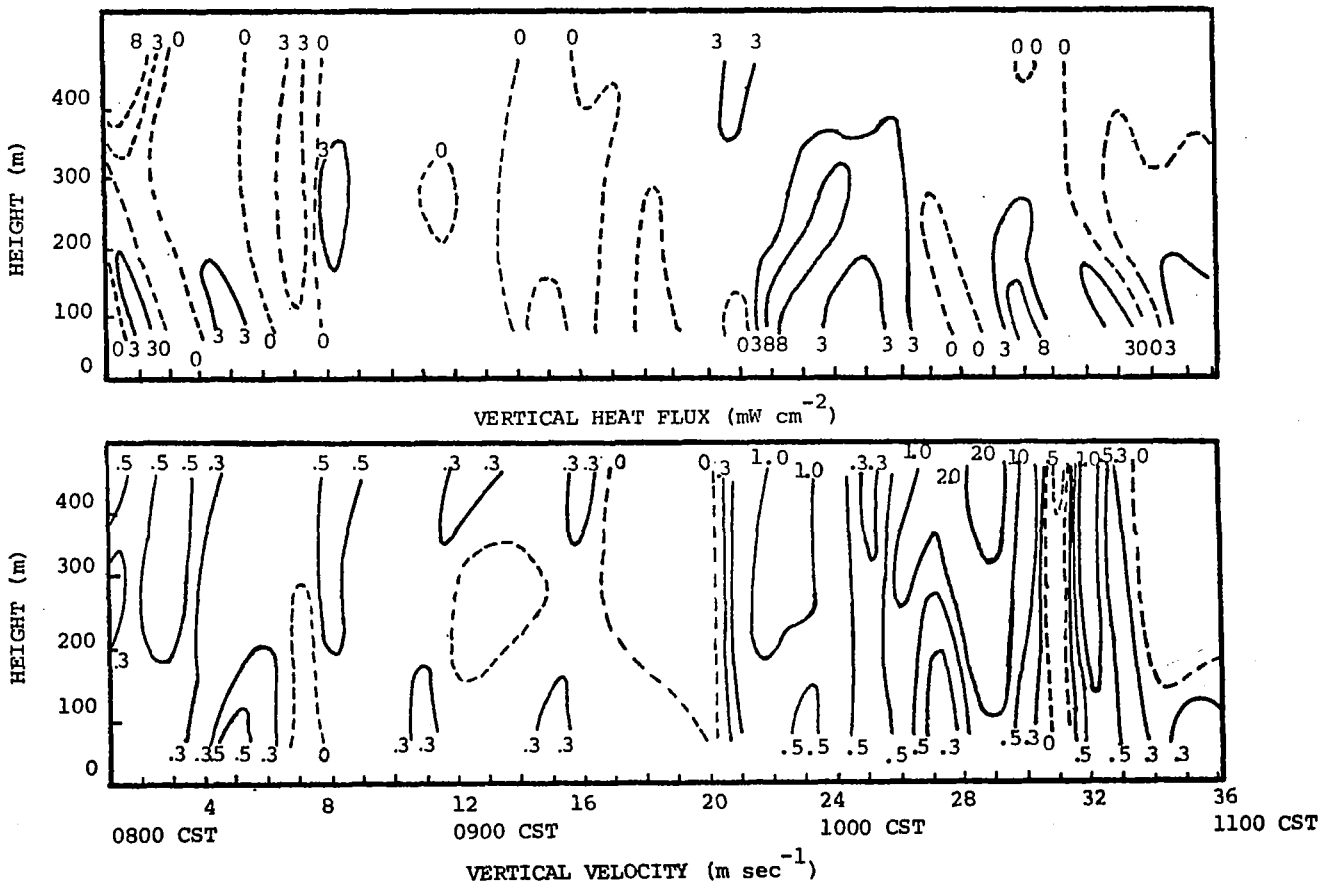

Fig. 7. Vertical velocity and vertical heat flux as a function of time and height for Data Set III. Period numbers are in the same manner as Fig. 5. Solid lines indicate positive vertical velocity (upward) and heat flux, dashed lines negative quantities.

mean wind direction, τ_{xz} at the surface equals τ_o and was determined from (8), while τ_{yz} is identically zero. The friction velocity, u_*, appearing in (8) was calculated from (7) by using the 1-hr mean, observed, wind speed at 26 m and a computed value of roughness length, z_o, for the area surrounding the tower. A method similar to that employed by Thuillier and Lappe (1964) was used to determine z_o (Fig. 9), in which the lower ends of the mean wind profiles intersect the ordinate at the value of z_o where the average wind speed equals zero. The value of 1.9 cm agrees well with the suggested value of around 5.0 cm for rough grass (Blackadar, Panofsky, and Fiedler, 1974).

The surface shearing stress of approximately 1.0 dynes cm^{-2} for all the averaging periods is in agreement with published figures, notably the direct (drag plate) measurement of 1.38 dynes cm^{-2} by Pasquill (1950) for rough grassland and comparable wind speed. The values of τ_o also agree with the general trends of the τ_{xz} profiles, except in the case of the third 15-min period where there is a strong transition over the lowest 26 m compared to an otherwise linear trend. The slope of this increase, however, is not greatly different from that of the first and fourth 15-min and 1-hr periods, so τ_o is not necessarily underestimated for this period.

Examination of Fig. 8 reveals:

(1) The values of τ_{xz} are comparable to those reported by other authors (Bradham, 1970; Campbell et al., 1956). The values of τ_{yz} near the ground agree with those published by Campbell et al., but they are an order of magnitude greater than those reported higher in the friction layer by Bradham or Charnock et al. This discrepancy may be linked to the fact that the observations in those two studies (test sites were located on the eastern coast of Florida and in the British West Indies, respectively) were made in air with a more stable lapse rate (4 to 9 deg C/km) than in the NSSL study over Oklahoma (slightly unstable). Lumley and Panofsky (1964) point out that lateral deviations are very sensitive to stability, particularly above the layer of strong

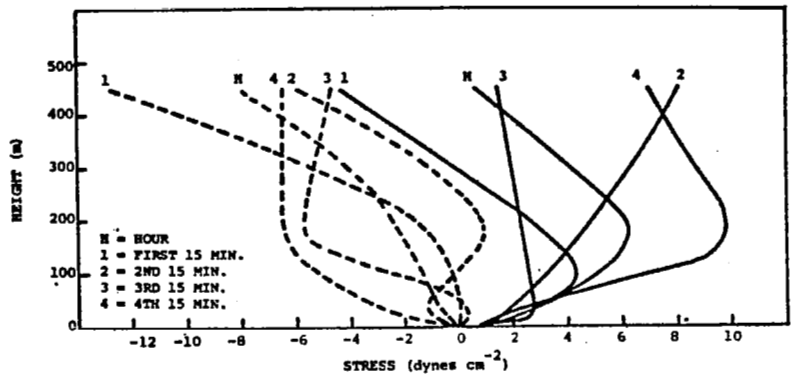

Fig. 8. Component shearing-stress profiles for the 15-min and 1-hr periods for Data Set I. Dashed lines refer to τ_{yz}, solid lines to τ_{xz}.

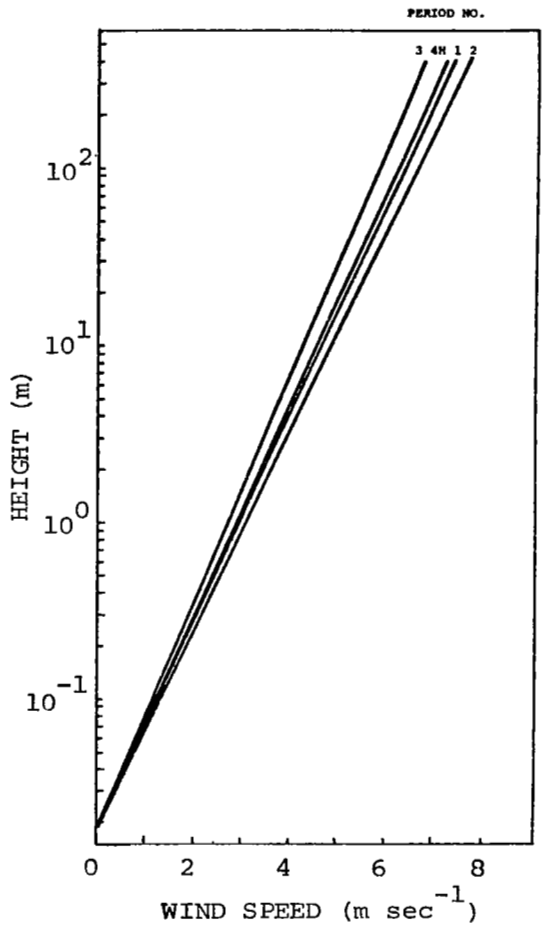

Fig. 9. Average wind speed profiles for the four lowest tower levels for Data Set I. Profiles for the fourth 15-min and 1-hr periods are the same.

wind shear adjacent to the surface.

(2) The variation with height of τ_{xz} is in general agreement with profiles presented in other studies. The 1-hr and 15-min mean profiles indicate that τ_{xz} becomes zero near the middle depth of the friction layer, as reported by both Bradham (1970) and Charnock et al. (1956). While both of these previous investigations favored a steady decrease with height of τ_{xz} from the surface, a fluctuation analysis by Charnock et al. of their data revealed a maximum value at around 200 m similar to those in Fig. 8; the authors explained its existence as due to the inability of the balloon to respond to the small-scale turbulent structure near the surface and, therefore, the increase of τ_{xz} to a low-level maximum merely reflected the exclusion of the contributions to the stress by the small eddies near the surface. The analysis of the NSSL tower data presented in this study, which includes the small-scale structure, and other recent tower studies (Campbell et al., 1970; Pena, Rider, and Armendariz, 1972), supports the actual existence of the low-level maximum. A comparison of the momentum flux per unit density, $-\overline{u'w'}$, from the 1-hr period of Set I, and a recent investigation by Pennell and LeMone (1974) in the fair-weather, trade-wind, friction layer by use of aircraft observations is presented in Fig. 10. The values of $-\overline{u'w'}_{max}$ from Set I and the trade-wind study are 0.55 and 0.20 $m^2\ sec^{-2}$, respectively. The similarity between the results of the two studies is remarkable, especially considering the difference between the two sites. Not only do the maxima occur at around the same height, but also the slopes of the sets of $-\overline{u'w'}$ values above and below the maxima are approximately the same. The profile for the second 15-min period of data Set I is somewhat peculiar, as it indicates either a steady increase of the shearing stress with height or a maximum at a much higher level than indicated by the other periods.

(3) The variation with height of τ_{yz} is in general agreement with that reported by Bradham and Charnock et al., as above, who indicate a general decrease with height from zero at the surface

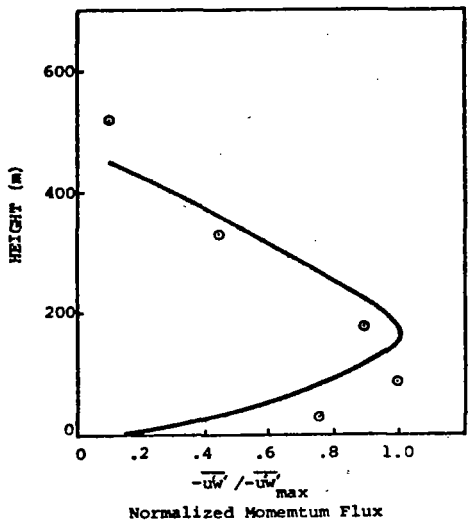

Fig. 10. Comparison of momentum flux as a function of height for Data Set I (solid line) and Pennell and LeMone (1974) (circles). See text for scaling values $-\overline{u'w'}_{max}$.

to a minimum at around 200 m. Profiles for the third and fourth 15-min periods are very close to this reported shape, while the profiles for the other periods indicate either minima at higher levels or a steady decrease in τ_{yz} with height. Again, the profile for the second 15-min period is somewhat peculiar.

(4) There is a noticeable similarity between the profiles of stress for the first and second and also the third and fourth 15-min periods, particularly in the set of τ_{yz} profiles. This feature may be better visualized in Fig. 11, in which the magnitude of the shearing-stress vector, $\vec{\tau}$, defined by

$$|\vec{\tau}| = [\tau_{xz}^2 + \tau_{yz}^2]^{\frac{1}{2}}, \qquad (14)$$

is plotted as a function of height. The values of $|\vec{\tau}|$ for the first two 15-min periods are seen to increase with height from the surface to 444 m, while the profiles of $|\vec{\tau}|$ for the last pair of 15-min periods show a maximum at around 200 m. The variation with height of shearing stress shows good correlation with

vertical motion (see Fig. 5), with the first two 15-min periods being dominated by downward motion and the third and fourth periods by upward motion.

The 1-hr values of $|\vec{\tau}|$ at 26,177, and 444 m from Fig. 11 are plotted in Fig. 12 on a semi-logarithmic scale. In the range from 26 to 444 m, $|\vec{\tau}|$ may be expressed to within 2 per cent by the relation

$$|\vec{\tau}| = 2.0 \ln\frac{z}{7.3} \qquad (15)$$

where z is the height above the ground in meters and the units of $|\vec{\tau}|$ are dynes cm^{-2}. This indicates that the magnitudes of both the shearing stress and the wind speed at a given height can be obtained from a logarithmic profile law. By dividing both sides of (15) by the surface shearing stress τ_o, one may obtain the non-dimensional form,

$$\frac{|\vec{\tau}|}{\tau_o} = 2.1 \ln\frac{z}{7.3} \quad , \qquad (16)$$

in which the units are the same as in (15).

Component shearing-stress profiles obtained from the two other data sets are shown in Fig. 13. In general, the curves are similar to those from Data Set I, (Fig. 8), except in the case of the first 1-hr profile from Set II. The momentum transport in the direction opposite that of the other 1-hr periods is linked to the presence of a temperature inversion during the first hour, a feature that will be examined later in the section dealing with average profiles of temperature. Another obvious feature of the profiles in Fig. 13 is the smaller magnitudes of the stresses as compared to Fig. 8. This is particularly true for the τ_{yz} values, which are known to increase with decreasing stability (Lumley and Panofsky, 1964). It already has been noted that, compared to Sets II and III, convection at the tower site was

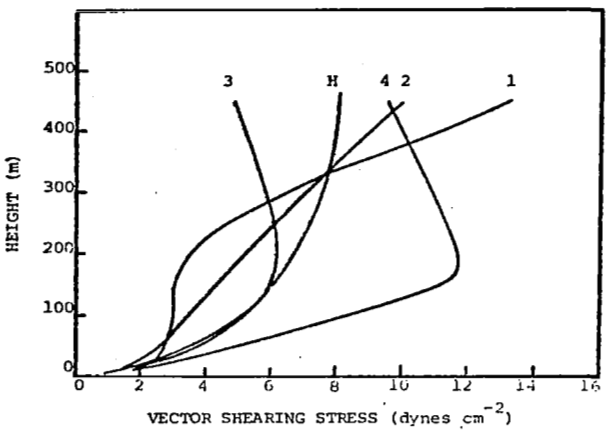

Fig. 11. Magnitude of the shearing-stress vector as a function of height for the 15-min and 1-hr periods for Data Set I. Profile labels are the same as in Fig. 8.

better developed when Data Set I was taken. Estimated values of the surface shearing stress, τ_o, from Fig. 13 are around 2 dynes cm^{-2} and agree both with published values and the results from Set I.

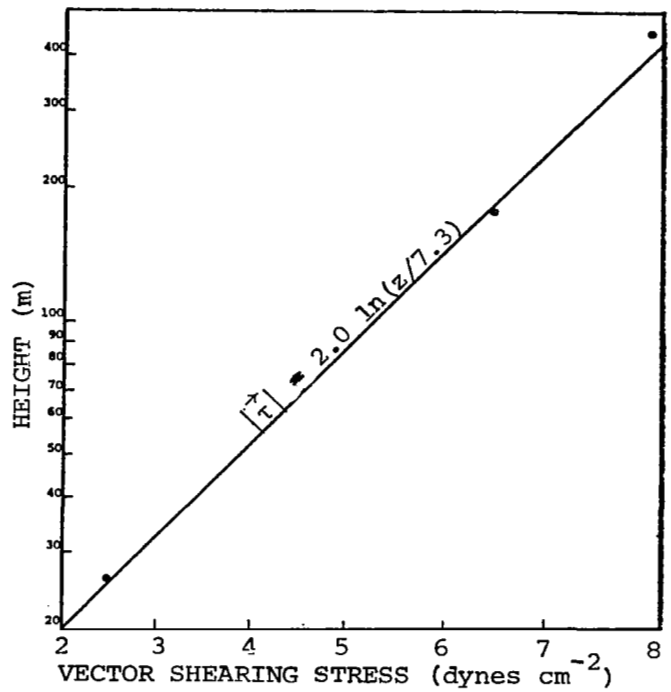

Fig. 12. Empirical relationship between the magnitude of the shearing-stress vector for the 1-hr period (see Fig. 11) and height.

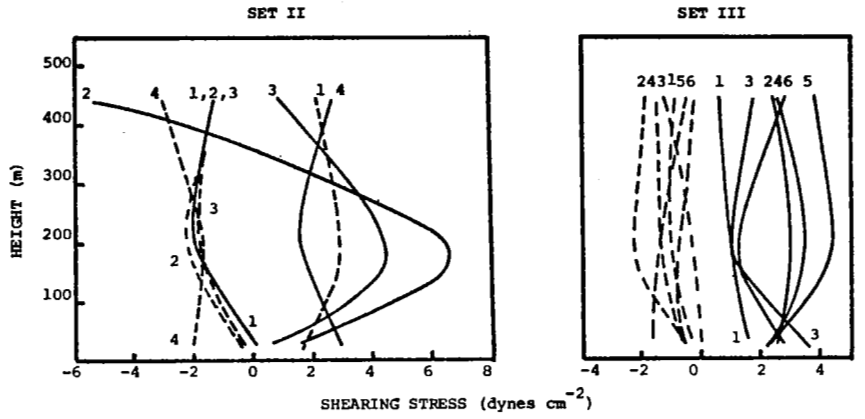

Fig. 13. Component shearing stresses for sequential 1-hr periods (Set II) and 30-min periods (Set III) as a function of height. Dashed lines refer to τ_{yz}, solid lines to τ_{xz}. Profile numbers refer to sequential averaging periods.

Five-minute means of the component shearing stresses from Set I are plotted in Fig. 14 in the same manner as vertical motion in Fig. 5, with Figs. 14a and 14b representing the fields of τ_{xz} and τ_{yz}, respectively. A regular periodic nature is exhibited by both components, with the period of the oscillations being approximately 20 min. Most notable in the figures is the apparent departure from a vertical structure that τ_{xz} makes below the 150-m level and the skewed structure of the τ_{yz} field, thereby indicating that τ_{xz} events near the surface preceed upper-level events, and than changes in τ_{yz} at a lower level lag those at a higher level.

The variation with height of 1-hr average, vertical, heat flux, H, given by (6) is shown in Fig. 15 for Data Set I. The values of H near the ground are comparable to those published by Campbell et al. (1970), viz., on the order of 1.0 mW cm^{-2} (10^4 erg cm^{-2} sec^{-1}). Direct measurements of heat flux above the surface boundary layer to which the values obtained in this study

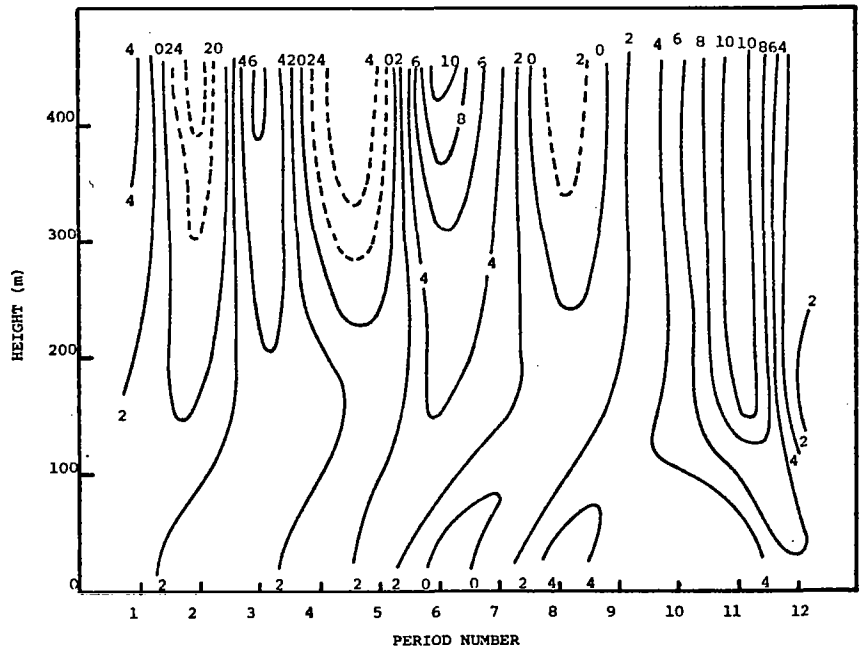

Fig. 14a. Component shearing stress, τ_{xz}, as a function of time and height for Data Set I. Solid lines refer to positive values, dashed lines to negative values, in dynes cm^{-2}.

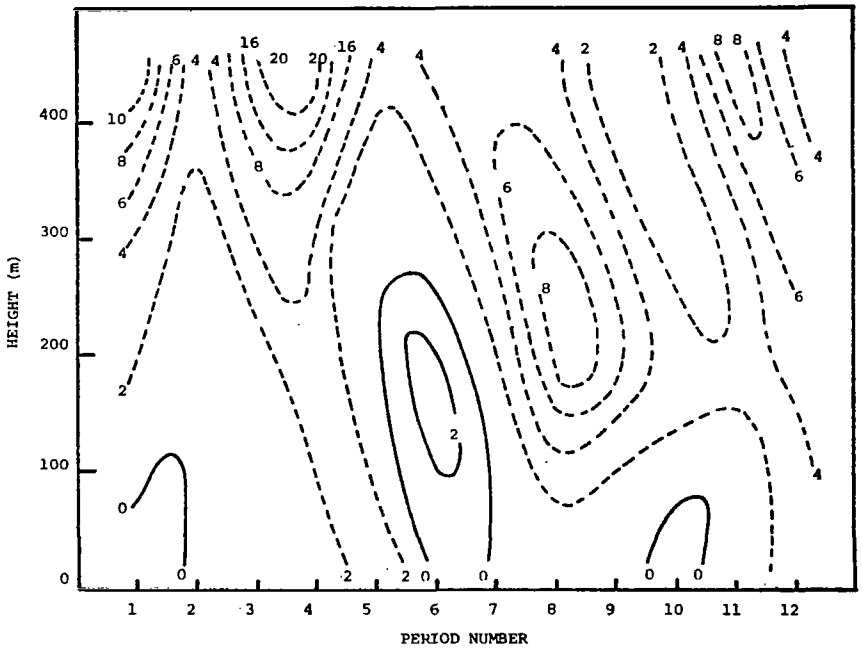

Fig. 14b. Component shearing stress, τ_{yz}, as a function of time and height for Data Set I. Solid lines refer to positive values, dashed lines to negative values, in dynes cm^{-2}.

may be compared could not be obtained, but the results of the study cited above indicate a general increase of H with height at least in the lowest levels during the early afternoon over open terrain. The 1-hr mean profile is approximately linear, and in the range from 26 to 444 m above the surface, H may be obtained from the relation,

$$H = 0.0097z + 0.1, \qquad (17)$$

in which z is the height above the surface in meters and the units of H are mW cm^{-2} (= erg cm^{-2} sec^{-1} X 10^{4}). The accretion of convection eddies above the surface described by Scorer and Ludlam (1953) may explain the increase in heat flux with height in that large eddies, because of their more orderly structure, are more efficient in transporting heat than smaller eddies.

Equation (17) may be made non-dimensional by dividing both sides by the quantity, $\bar{\rho}C_p T_o^* u_*$, in which $\bar{\rho}$ is the air density, C_p the specific heat of dry air at constant pressure, T_o^* the surface scaling temperature, and u_* the friction velocity. The magnitude of T_o^*, a constant for logarithmic wind profiles, can be obtained from the definition (Pena et al., 1972),

$$T_o^* = \frac{1}{ku_*} \frac{H_o}{\bar{\rho}C_p} \quad , \qquad (18)$$

where H_o is the vertical heat flux at the surface and k is von Karman's constant (usually ascribed the value 0.4). Thus (17) takes on the non dimensional form

$$\frac{H}{\bar{\rho}C_p T_o^* u_*} = 3.88z + 0.4 \quad , \qquad (19)$$

in which the units of z are cm and H is in erg cm^{-2} sec^{-1}.

Profiles of vertical heat flux for sequential periods of 1 hr from Set II are shown in Fig. 16. The values of H in the figure generally are comparable to those derived from Data Set I, except in the case of the first hour period for which the heat-flux

values are twice the magnitude of those from both Set I and the other periods from Set II. An explanation of this will be presented in the section concerning temperature profiles.

The field of vertical flux derived from 5-min averages of H from Set I is shown in Fig. 17, which indicates a periodic structure similar to that of mean vertical motion. Approximately the first half of the hour period is dominated by negative heat flux, the second half by positive heat flux. The anomaly between the 5-min and 1-hr mean temperatures is shown in Fig. 18, which indicates warmer air temperatures associated with the positive heat flux and cooler air temperatures with negative heat flux. There is an indication in Fig. 18 of a return of cooler temperatures at the end of the hour, so that the figure represents a regime of

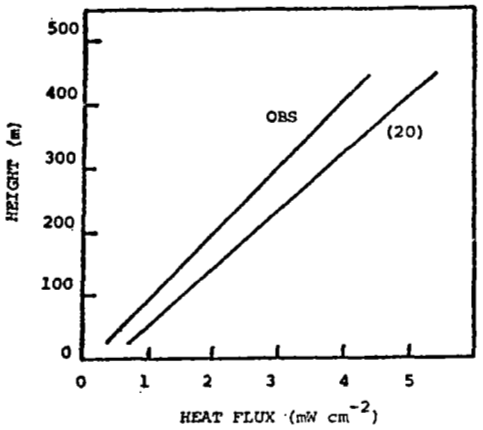

Fig. 15. Profiles of vertical heat flux for the 1-hr period for Data Set I. Hour profile labelled (20) was determined from equation (20) and is discussed later in the text.

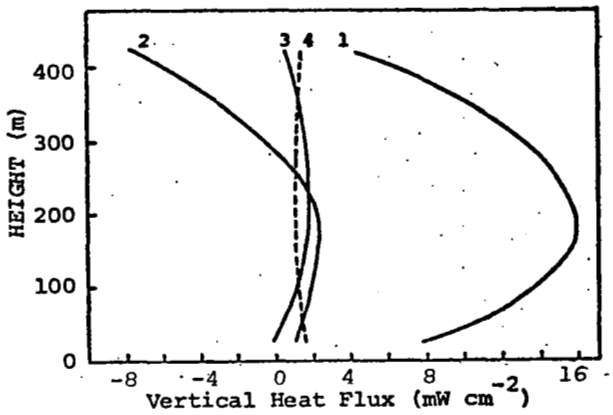

Fig. 16. Profiles of vertical heat flux for sequential 1-hr periods for Data Set II.

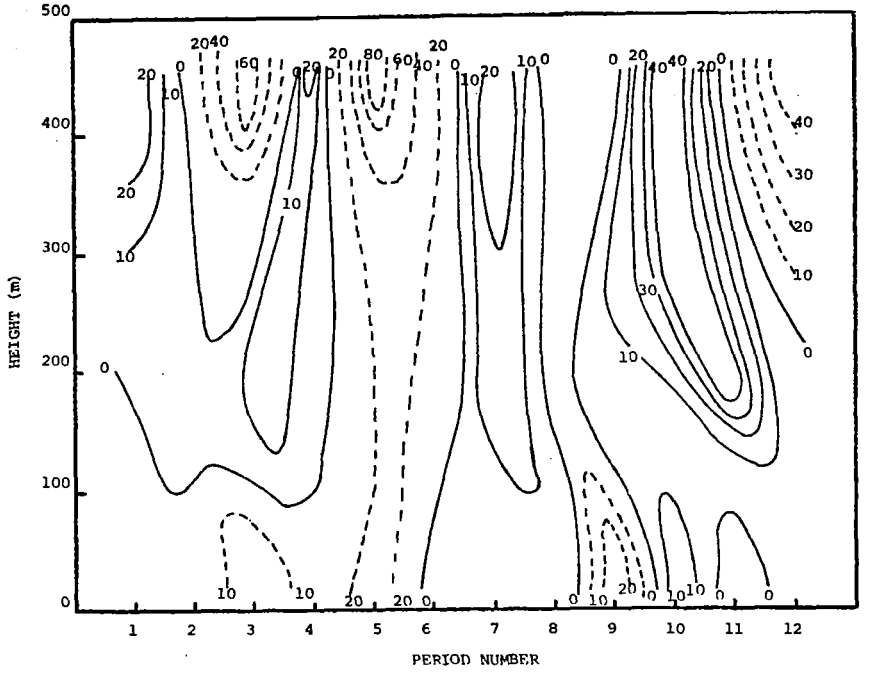

Fig. 17. Vertical heat flux as a function of time and height for Data Set I. Solid lines refer to positive values, dashed lines to negative values, in mW cm^{-2}.

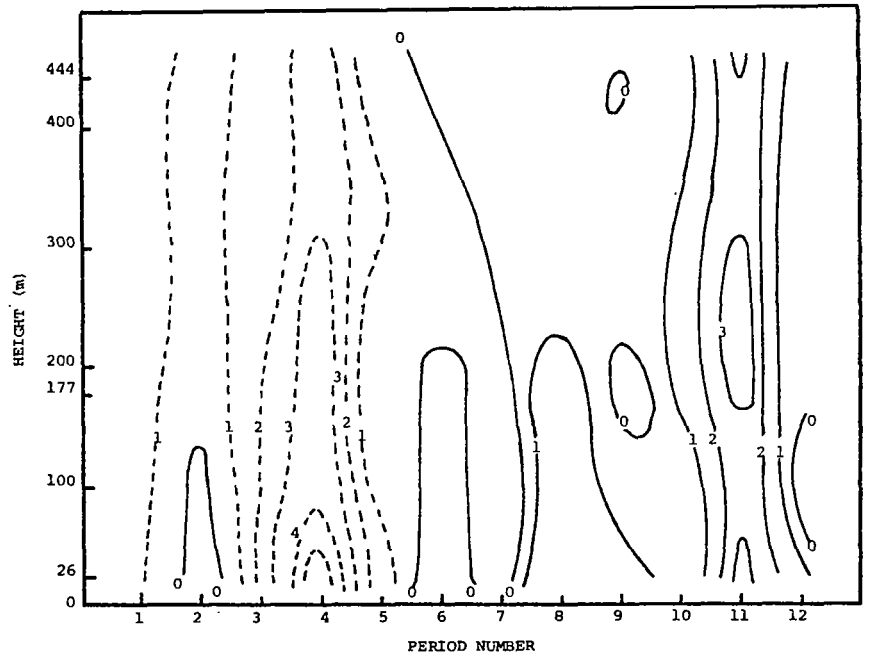

Fig. 18. Difference between 5-min and 1-hr average temperature as a function of time and height. Solid lines indicate the 5-min mean temperature to be warmer than the 1-hr mean value at that level; dashed lines indicate cooler temperatures, in degrees Celsius.

periodic anomaly and not just a steady increase in air temperature through the hour (which also would show roughly the first half of the hour cooler and the second half warmer than the 1-hr mean temperature).

The variation of vertical heat flux with time and height for Set III is shown in Fig. 7 in a manner similar to Fig. 17 for Set I. Positive values of H are seen to dominate the 3 hr of the data set, but large values of positive H do not appear until the latter half of the data period. This correlates with the larger values of vertical velocity appearing in this segment of the set (see Fig. 7). Large values of negative heat flux appear only in the first hour. The correlation between individual maxima and minima of H and vertical motion in Fig. 7 is not as good as in the figures dealing with Set I. Again, the less-developed nature of the convective regime may explain this.

C. Mean Wind and Temperature Profiles

Hour and 15-min average temperature profiles for Data Set I are shown in Fig. 19. There is little variation between the values of environmental lapse rate, γ, for the four 15-min periods, with γ being approximately 10.77 deg C km^{-1} over the tower height, except in the case of the second 15-min period for which the value of γ is 10.53 deg C km^{-1}. The value of the 1-hr mean lapse rate is also 10.77 deg C km^{-1}, thus exceeding the dry adiabatic lapse rate by approximately 1 deg so that the layer between 26 and 444 m is slightly superadiabatic. The slight deviation of the temperature profiles from a linear form toward warmer temperatures near the surface indicates that the layer below 26 m is almost certainly superadiabatic also, especially in light of the clear sky conditions leading to strong insolation. Because vertical heat flux is zero when γ is only 70 to 80 per cent of the dry adiabatic lapse rate, the large values of H presented in the previous section are consistent with the existing lapse rates, and it is reasonable to assume that some form of convective activity must exist at the sampling time acting to reduce the instability (Lumley and Panofsky, 1964). Scorer and Ludlam (1953) point out that the

removal of heat from the surface is enhanced by the presence of wind which acts to encourage the growth of large convective eddies.

The average temperature profiles in Fig. 19 may be used to estimate values of the vertical heat flux, H, for the hour of observations comprising Data Set I. Heat flux may be related to the change with time of temperature at a level by the equation (Lenschow, 1974),

$$H = \bar{\rho} C_p \frac{\partial T}{\partial t} z + H_o \quad , \qquad (20)$$

in which $\bar{\rho}$ is the average air density, C_p the specific heat of dry air at constant pressure (taken as 9.96×10^6 cm^2 sec^{-2} deg^{-1}), $\partial T/\partial t$ the temperature change, z the height, and H_o the heat flux at the surface. This equation is of the same form as (14), so when z = 0, the surface heat flux H_o must be approximately 0.1 mW cm^{-2} (= 10^3 erg cm^{-2} sec^{-1}). Substituting this and appropriate values of the dependent variables from the analysis of Set I, one may solve (20) to produce a profile of H comparable to the 1-hr profile presented in Fig. 15. The two profiles are seen to agree fairly well. The coefficient of z in (17) is close to the value of $\bar{\rho} C_p \frac{\partial T}{\partial t}$ in (20), viz., 0.0097 and 0.015, respectively.

Average temperature profiles for Data Sets II and III are shown in Fig. 20, which indicates a transition in the lapse rate at the tower site through the sampling periods. The first 1-hr period from Set II, centered at 1230 CST, clearly shows an inversion below the 266-m level, presumably associated with the presence of the anticyclonic system. The inversion must have been very strong during the earlier hours, as evidenced by its presence in the early afternoon. By the next time period, however, the inversion had dissipated and temperature lapse rates had become roughly adiabatic. A representative heat flux over the hour in which the inversion dissipated can be obtained from the relation (Lenschow, 1974),

$$H = \bar{\rho} C_p \frac{\partial T}{\partial t} z \quad , \qquad (21)$$

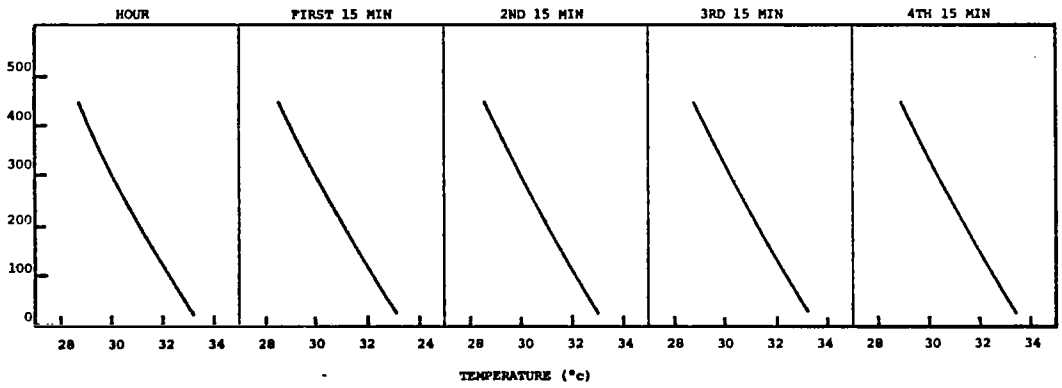

Fig. 19. Average temperature profiles for the 15-min and 1-hr periods for Data Set I.

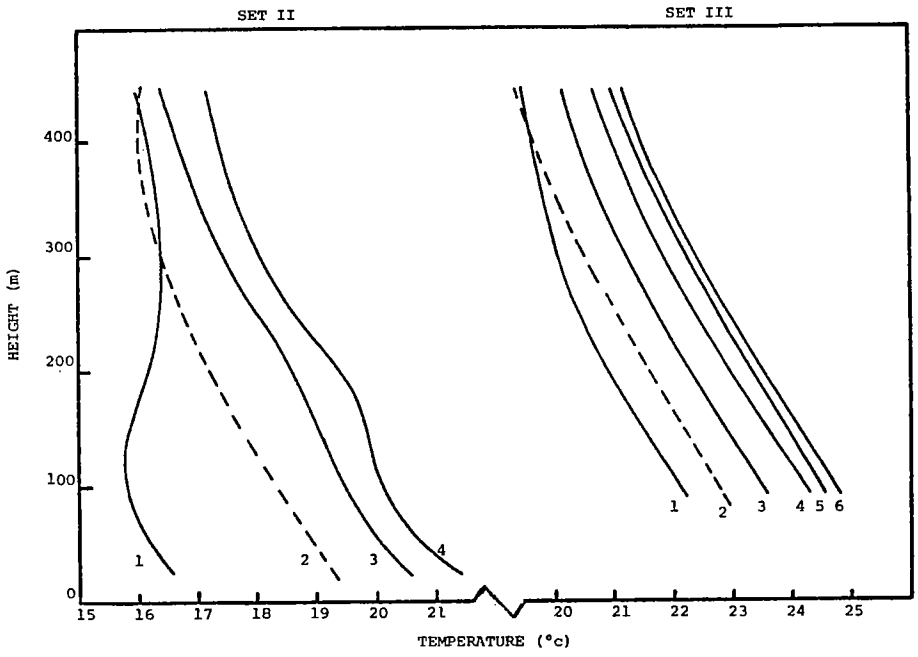

Fig. 20. Sequential average temperature profiles for Data Sets II and III. For Set II the averaging period was 1 hr, while for Set III the period was 30 min.

which neglects the heat flux at the surface. Solution of (21) with values for the dependent variables taken from the analysis of Set II, gives a value of around 8 mW cm^{-2} for H at the 100-m level, which is a comparatively large value relative to those from Set I at the same height. A large value of H would be expected, though, and referral to Fig. 16 shows a value of approximately 13 mW cm^{-2} at this level. The difference between these two values can be attributed partially to the surface heat flux, H_o, neglected in (21), which would tend to make the value of H from Fig. 16 larger than that calculated from (21) under the conditions at the tower site (it is unlikely that H_o would be negative at this time of day). The previously-noted fact that the profile of H from the first 1-hr period constitutes greater values than the three later profiles in Fig. 16 can be attributed to the heat flux leading to the dissipation of the inversion. Another interesting feature of the heat-flux and temperature profiles is the agreement between the negative heat flux and the cooler temperatures in the upper regions for the second period of Data Set II.

The results of the analysis of Set III are similar to that of Set II. There is some indication in Fig. 20 of the presence of a temperature inversion prior to the first 30-min period. In fact, analysis of the first 5 min of the data shows an inversion. The later temperature profiles are approximately adiabatic and appear very uniform although one must keep in mind that temperature data were obtained at only three levels in Set III.

Profiles of 15-min and 1-hr mean wind speed from Set I are shown in Fig 21. Each profile of observed speed is accompanied by a logarithmic profile calculated by using (7) with z_o = 1.9 cm and u_* determined from the observed wind speed at the 26-m level for each period. The log-law fit to the 15-min mean profiles is very good up to at least 200 m, and up to 444 m there is no deviation from the log-law profiles greater than 1.0 m sec^{-1}. In the upper region where deviations occur, the observed values

are less than the theoretical values for the first two periods and greater for the second two periods, again being correlated with the field of vertical motion. The 1-hr mean wind-speed profile approximates the logarithmic profile to a high degree throughout the tower height. The approach of observed wind speed profiles to a logarithmic profile at heights well above the surface boundary layer has been reported by Thuillier and Lappe (1964) and Carl et al. (1973), but only under near-neutral conditions. When convection prevails, the variation of wind speed with height should be proportional to $z^{-1/3}$ and not ln z (Lumley and Panofsky, 1964), which is not indicated in Fig. 21.

One-hour and 15-min, average, component, wind-velocity profiles along the longitudinal and lateral axes are shown in Figs. 22a and 22b, respectively, with the longitudinal axis parallel to and the lateral axis perpendicular to the 1-hr mean surface wind direction. The data show a deviation at the 444-m level of only 7 deg from the mean surface wind direction, but a turning of the velocity vector with height in the manner of the Ekman spiral is apparent although the magnitude of the angular deviations is

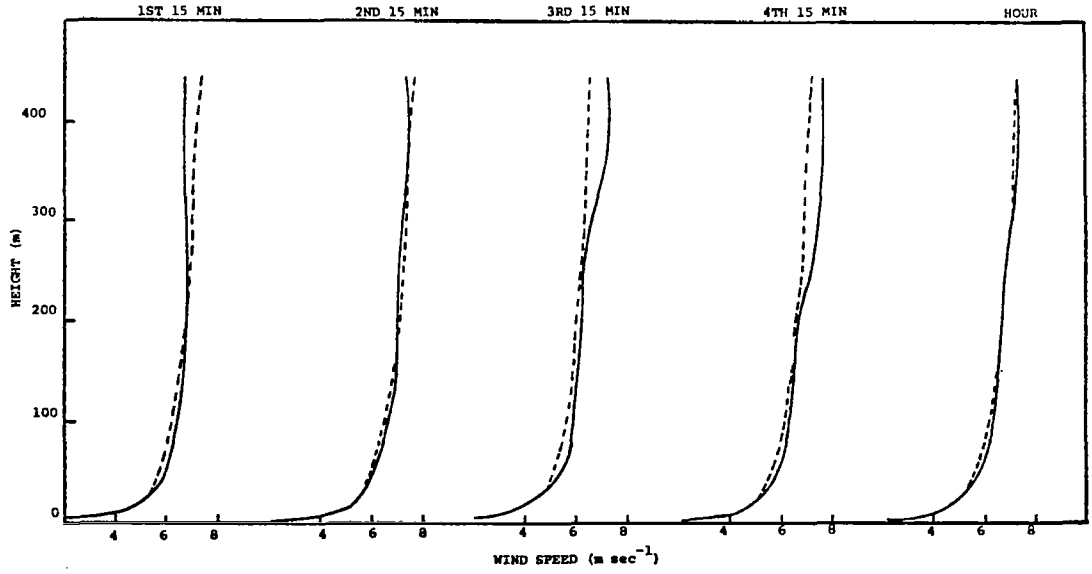

Fig. 21. Mean wind speed profiles for the 15-min and 1-hr periods for Data Set I. Dashed lines represent theoretical logarithmic profiles for each period (see text).

much smaller than that predicted by theory. Thus, the shearing stress obviously could not be constant over the height of the tower, a fact already evidenced by observations (Fig. 11).

The profiles in Fig. 22a approximate logarithmic curves with the 15-min values clustered about the 1-hr profile. The similarity between the first and second and the third and fourth 15-min profiles of mean lateral wind velocity (Fig. 22b) is evident as it was for vertical motion and shearing stress.

Profiles of 1-hr mean wind speed and direction from Set II are shown in Fig. 23. The low-level speed maximum associated with the temperature inversion of the first hour period is present, along with the large turning of the wind vector with height below the inversion. Unlike the wind profiles from Set I (see Fig. 21), the variation of wind speed with height in Fig. 23 deviates significantly from that prescribed by the logarithmic law (7). It may be noted that the observed mean profile approaches more closely the theoretical log-law profile towards the later part of Set II, presumably as the effects of the dissipation of the inversion diminish and the layer approaches a more thoroughly-mixed state.

An attempt was made to correct for the effects of stability changes on the 1-hr mean wind profiles by use of the log-linear profile law (Munn, 1966),

$$\bar{V} = \frac{u_*}{k}\left[\ln \frac{z}{z_o} + \psi\left(\frac{z}{L}\right)\right] \quad ; \quad z \gg z_o \quad , \tag{22}$$

in which u_*, k, z, and z_o are the same as in (7) and $\psi(zL^{-1})$ a stability correction that is a function of non-dimensional height, zL^{-1}. The Monin-Obukhov length, L, contains the ratio of the exchange coefficients of heat and momentum, so to facilitate calculation, (22) may be re-written

$$\bar{V} = \frac{u_*}{k}\left[\ln \frac{z}{z_o} + \beta\left(\frac{z}{L},\right)\right] \quad , \tag{23}$$

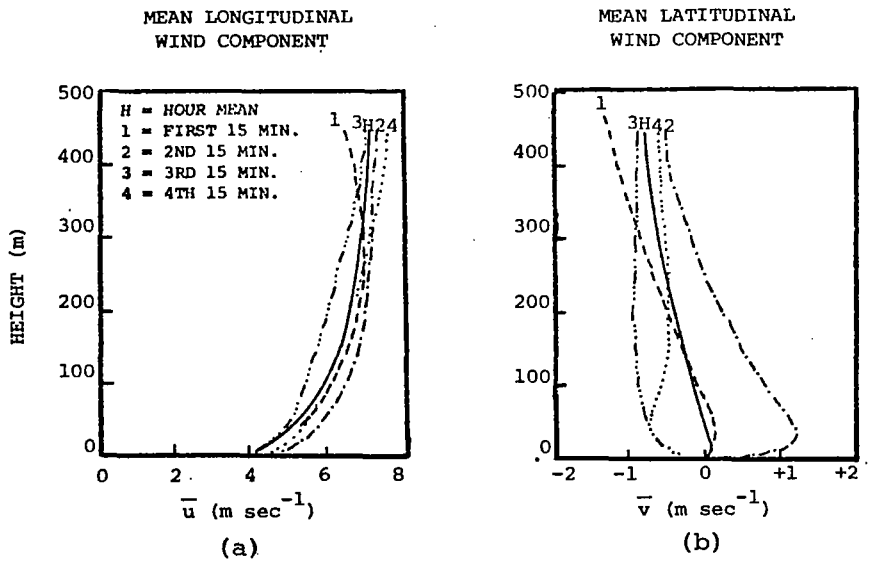

Fig. 22. Mean longitudinal and lateral velocity profiles for the 15-min and 1-hr periods for Data Set I.

where the stability correction function has been replaced by a constant times the ratio of height, z, to the modified Monin-Obukhov length, L . The empirically-derived value of β now contains the effect of the ratio of the exchange coefficients. The modified Monin-Obukhov length is defined by (Munn, 1966) as

$$L' = \frac{-u_*^3 C_p \bar{\rho} \bar{T}}{kgH} \tag{24}$$

in which T is the mean temperature for the period, g the acceleration due to gravity (980 cm sec^{-2}), and the remaining symbols are as in previous equations. To solve (23) for the wind speed, $\bar{V}$, values of u_* were calculated by using (7) at the 26-m level for each hour period. Then, (23) was solved for β at the 177-m level from known values for the other variables. Finally, with the computed values of β for each period, (23) was solved for $\bar{V}$ at the 444-m level; the results are shown in Table 4. Although the

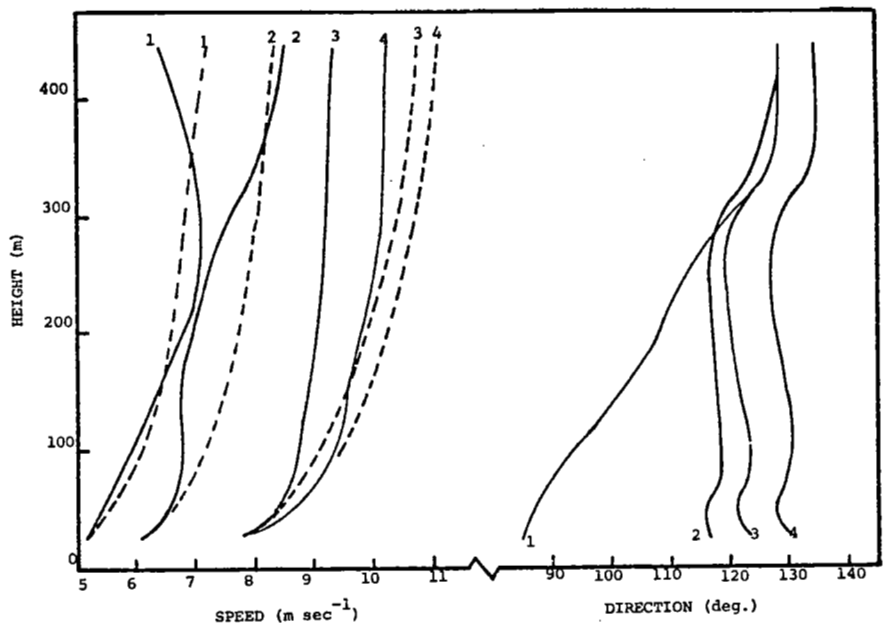

Fig. 23. Sequential 1-hr mean profiles of wind speed and direction for Data Set II. Dashed lines represent logarithmic profiles for each period, as in Fig. 21.

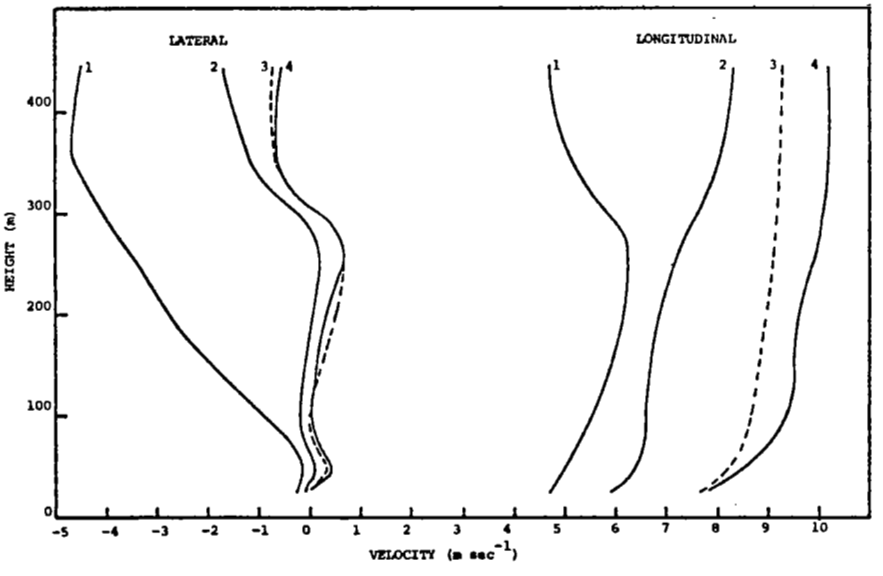

Fig. 24. Sequential 1-hr mean profiles of the longitudinal and lateral components of horizontal wind velocity for Data Set II.

Table IV

Results of the calculation of $\overline{V}$ at the 444-m level for Set II

Period	u_* (cm sec^{-1})	z/L'	β	$\overline{V}$ calculated (m sec^{-1})	$\overline{V}$ observed (m sec^{-1})	$\overline{V}$ log-law (m sec^{-1})
1	29.28	-8.8	-.02	7.3	6.5	7.15
2	34.12	10.1	0.74	14.7	8.5	8.35
3	44.07	-0.4	1.93	9.9	9.3	10.75
4	45.21	-0.8	1.77	9.5	10.3	11.10

values of $\bar{V}$ calculated from (23) do not necessarily approximate the observed values of $\bar{V}$, use of (23) did effectively indicate whether the value of mean wind speed would be greater or less than the log-law estimate of $\bar{V}$, except in the case when the temperature inversion was present below the 444-m level (first hour period). This method of solution assumes β and the ratio of the exchange coefficients of heat and momentum to be constant through the height of the tower, which are questionable assumptions even without the presence of a temperature inversion.

Mean longitudinal and lateral wind components for the sequential 1-hr periods of Set II are presented in Fig. 24, which shows that the lateral component makes a significant contribution to the vector wind speed only in the case of the first 1-hr period.

The differences between 5-min and 1-hr average longitudinal wind speed as a function of time and height for Set I are shown in Fig. 25. The anomalies represent the larger-scale turbulent circulations at the tower site superimposed on the prevailing wind as a result of the overall synoptic conditions. Once again, the anomalies do not represent large eddies themselves but rather indicate the character of the turbulence over time and space on the large scale, thereby providing a pseudo-Lagrangian view of the local wind structure. The regular recurring nature of the with- and against-mean flow segments is visible, with the period of the oscillations being around 20 min. The regions between successive anomalies represent local areas of divergence and convergence, and, therefore, should be correlated to some degree with the local field of vertical motion. Comparison of Fig. 5 to Fig. 25 shows that areas of divergence and convergence are associated with areas of downward and upward motion, respectively. It may be noted that in regions lacking a change in the local longitudinal wind structure there is also little change in the vertical motion field (the eighth 5-min period for example).

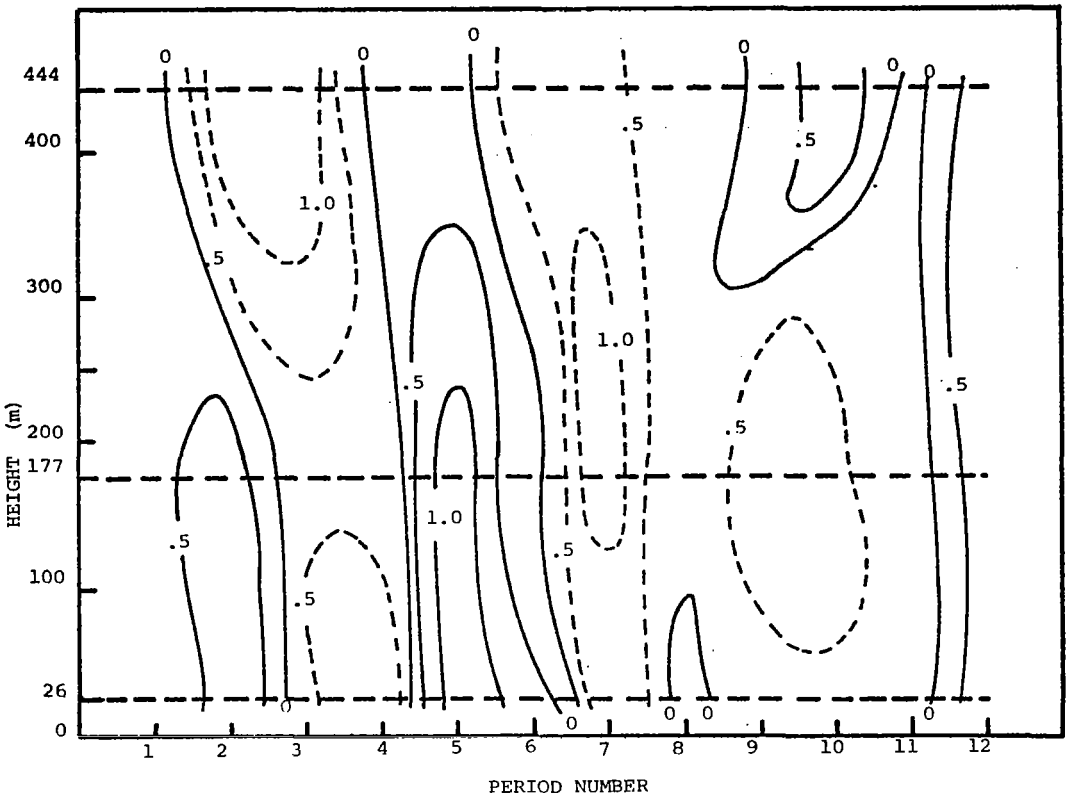

Fig. 25. Difference between 5-min and 1-hr mean longitudinal wind velocity as a function of time and height. Hourly mean flow is from right to left in the figure. Solid lines indicate 5-min mean flow greater than 1-hr mean flow, dashed lines indicate less than 1-hr mean flow, in m sec^{-1}.

D. Evaluation of the Exchange Coefficient Hypothesis

The capability of calculating the shearing stresses directly from covariances allows an accurate determination of the momentum exchange coefficient, K, at several levels above the surface. This makes possible a comparison of K values determined by two independent methods and a check of the validity of the exchange

coefficient hypothesis.

To simplify the analysis, the 1-hr, mean, component, wind-velocity profiles from Data Set I (Fig. 22) were used. It was found that the longitudinal component could be approximated to within 2 per cent through the height interval 26-444 m of the tower by the empirical expression

$$\bar{u} = 61.04 \ln z, \qquad (25)$$

in which $\bar{u}$ is the 1-hr, mean, longitudinal, wind component in cm sec^{-1} and z is the height in cm. Thus, the longitudinal component of the shear of the mean wind $\partial u(\partial z)^{-1}$ could be determined easily as given by

$$\frac{\partial \bar{u}}{\partial z} = \frac{61.04}{z}, \qquad (26)$$

where the units of shear are sec^{-1}.

From the values of the component shearing stresses shown in Fig. 8 and component wind shears from (26), the momentum exchange coefficients can be determined directly by using (9) and (10). In this method, which shall be referred to as the fluctuation method, $\bar{\rho}$ takes the value of 1.11×10^{-3} gm cm^{-3} and is taken to be invariant through the tower height.

In the layer in which the logarithmic wind profile law is applicable, the exchange coefficient can be determined as follows. By differentiating the log law (7) with respect to z and making substitutions from (8) and (9) -- in this case τ_{xz} is the same as τ_o, one can express the momentum exchange coefficient as (Munn, 1966)

$$K_{xz} = u_* kz, \qquad (27)$$

where u_* is the friction velocity, k the von Karman constant, and z the height. From the values in Fig. 8, u_* for the 1-hr period is found to be 29.0 cm sec^{-1} by use of (8). The von Karman constant usually is ascribed the value 0.4 (Lumley and Panofsky, 1964).

The results of these methods are shown in Fig. 26. The log-law method approximates the value of K_{xz} obtained from the fluctuation method fairly well near the surface. Above 26 m the two methods tend to handle the variation with height of the exchange coefficient differently, with the log-law method showing a steady increase with height, and the fluctuation method an increase to a maximum at 250 m. From (9), K_{xz} for a logarithmic wind profile should increase with height provided the stress remains the same. The decrease with height above 250 m indicated by the fluctuation method reflects the simultaneous decrease in both the shear and stress so that K_{xz} approaches zero near the top of the tower. The results of the study by Charnock et al. (1956) are shown in Fig. 26, which indicates that their findings are similar to the product of the log-law method up to the maximum at 300 m. Also shown in the figure is the variation with height of the exchange coefficient of momentum obtained by Blackadar and Panofsky (1969) using a modified geostrophic departure method; a low-level maximum is exhibited at about the same level as indicated by the fluctuation method.

E. Wind Shear

The results of a statistical examination of wind shear at the NSSL facility are shown in Figs. 27a and 27b, constructed from cumulative frequency diagrams of scalar wind shear build-up to 444-m for Data Sets I and II. Because it includes observations from only three levels on the tower, Set III was not used in this analysis. The figures were prepared from values of scalar wind shear, $|\Delta\bar{V}|(\Delta z)^{-1}$, computed for each observation over the entire collecting period, so that a comparable number of observations were used in constructing each figure. The intervals over which the shear was computed were 89, 178, 276, 354, 399, and 418 m, from the top of the tower downward. Thus, the shears represent those building up to the wind speed at the top of the tower. Examination of the curves in Figs. 27a and 27b reveals them to be very similar.

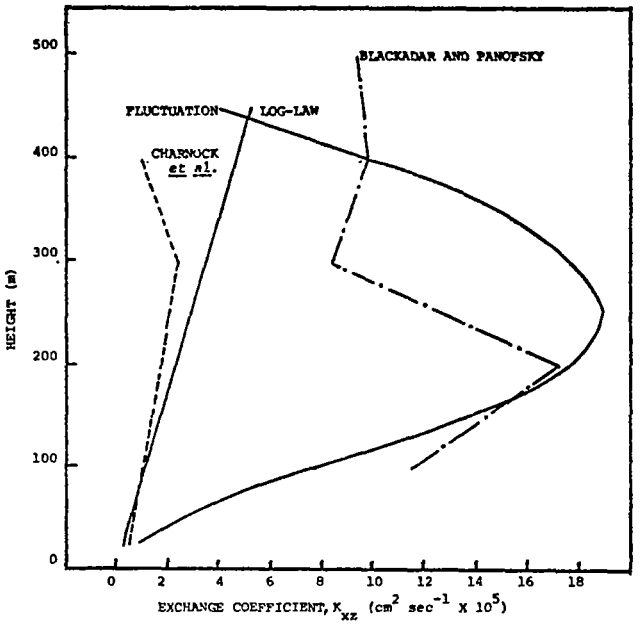

Fig. 26. Variation with height of the momentum exchange coefficient as determined by two independent methods. See text for explanation of methods. Dashed line represents calculation of K_{xz} by Charnock et al. (1956), dash-dot line represents results obtained by Blackadar and Panofsky (1969).

F. The Magnitude of Turbulent Fluctuations

The variation with height of the longitudinal and lateral components of variance for the 15-min and 1-hr periods of Data Set I are shown in Fig. 28, and for sequential 30-min periods of Data Set III in Fig 29. The longitudinal component, σ_u^2, and lateral component, σ_v^2, are shown in Figs. 28a and 28b, respectively, while the sum of σ_u^2 and σ_v^2 is shown in Fig. 28c. While σ_v^2 shows no systematic variation with height, σ_u^2 exhibits a general decrease with height for all periods, a feature previously noted by Blackadar et al. (1974). An interesting and as yet unexplained feature of both Figs. 28a and 28b is the divergence of the profiles between the 100- and 200-m levels. In Fig. 28c, the combined variance profiles remain in a fairly coherent group through the tower height, except in the case of the first 15-min period, which shows much smaller values in the middle region of the tower height.

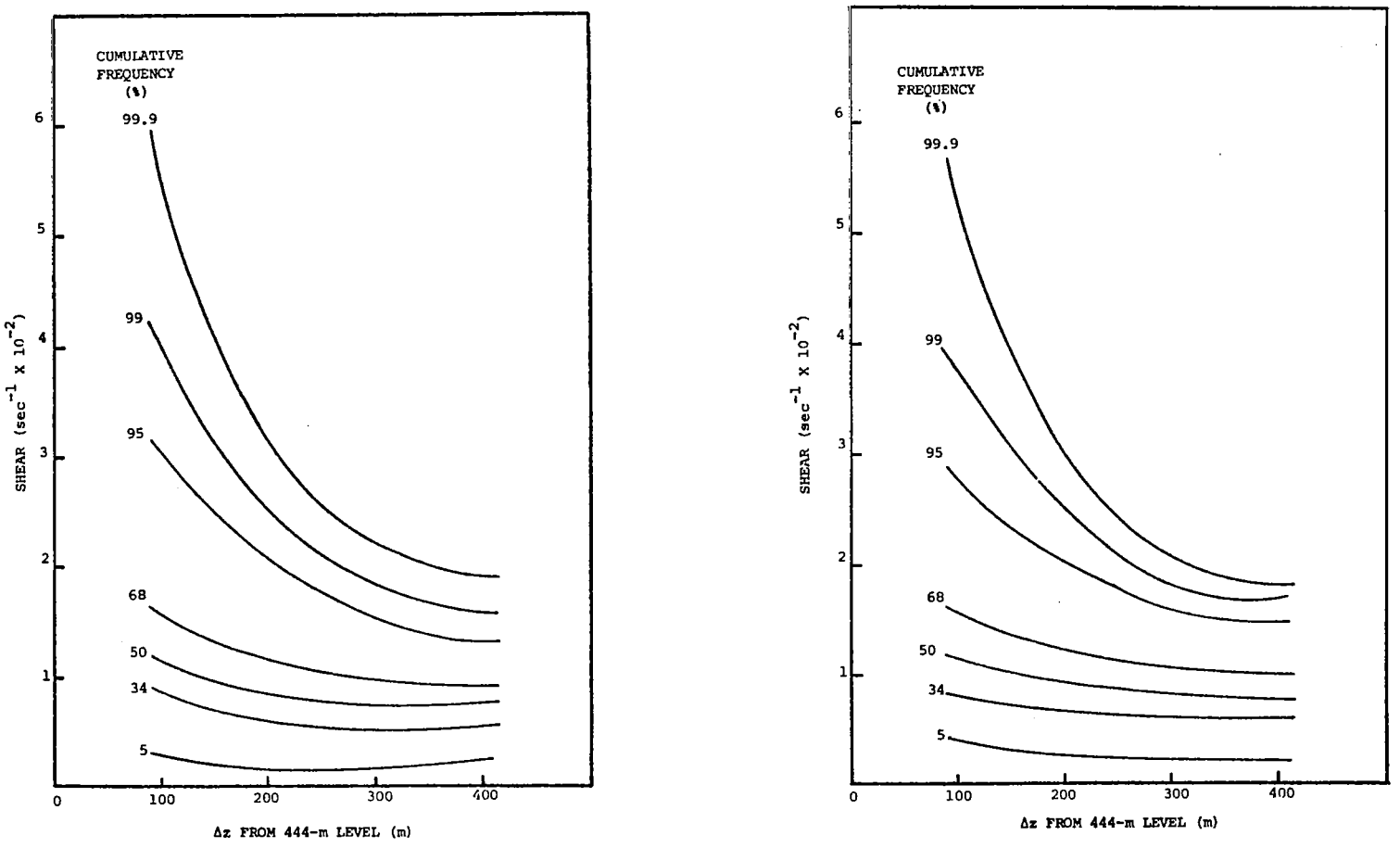

Fig. 27. Cumulative frequency diagrams of scalar wind shear build-up to the wind speed at the top of the tower for Data Sets I (a) and II (b). Time period for (a) was one hour (1793 observations) and for (b) four consecutive hours (1439 observations).

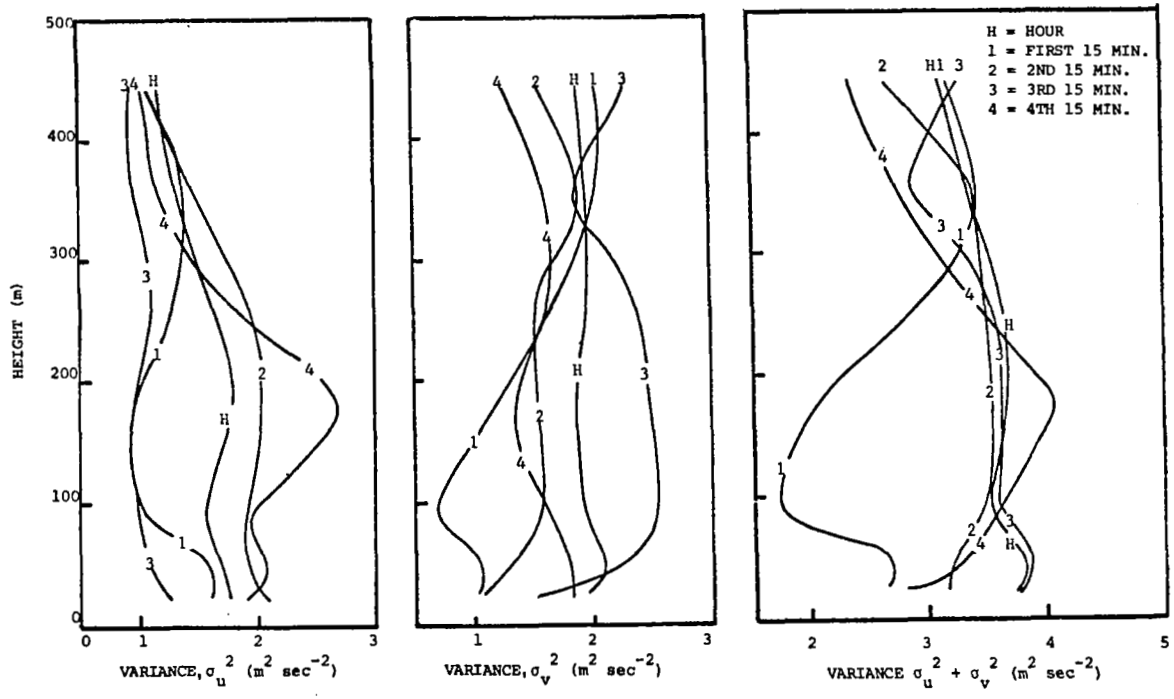

Fig. 28 Profiles of the longitudinal and lateral components of variance and the sum of the longitudinal and lateral components of variance for the 15-min and 1-hr periods for Data Set I.

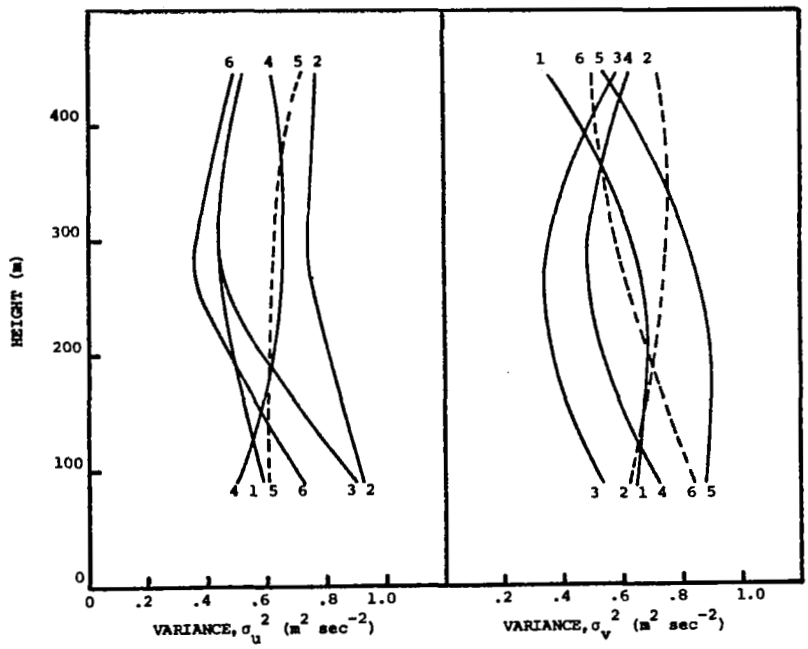

Fig. 29. Profiles of the longitudinal and lateral components of variance for sequential 30-min periods for Data Set III. Profile numbers refer to sequential averaging periods.

Lumley and Panofsky (1964) state that the standard deviations of the horizontal component velocities, σ_u and σ_v, should be proportional to the friction velocity, u_*, and give values of the ratio, $\sigma_v u_*^{-1}$, that range from 1.3 to 2.6 for various locations. Blackadar *et al.* (1974), from their study for Cape Canaveral, recommend that the values of $\sigma_u u_*^{-1}$ and $\sigma_v u_*^{-1}$ are approximately 2.5 and 2.2, respectively, where u_* is measured at a low level. A recent study by Pennell and LeMone (1974) shows values of $\sigma_u u_*^{-1}$ and $\sigma_v u_*^{-1}$ that range from 1.5 to 4.0, and 1.5 to 2.5, respectively, in the lower 400 m of the fair-weather, trade-wind, friction layer. Table V gives values of the two ratios computed from the four sequential hour segments of Data Set II. The entire range of harmonics made contributions to the variances over the 1-hr periods,

TABLE V

Ratios of the standard deviations of component velocities to the friction velocity for sequential hour periods from Data Set II

Period	u_* (m sec^{-1})	σ_u/u_*	σ_v/u_*	σ_w/u_*
1	0.29	3.40	7.08	1.42
2	0.34	3.53	3.15	1.33
3	0.44	3.18	2.37	1.07
4	0.05	3.45	2.76	1.40

and while the ratio, $\sigma_u u_*^{-1}$, remained roughly constant over the four periods, the ratio, $\sigma_v u_*^{-1}$, decreased with time from an extremely large value (7.08) for the first period, which was dominated by the temperature inversion. Although the values of the ratios in Table V are larger than the suggested values, most are within the ranges observed by Pennell and LeMone (1974). From the 1-hr values in Figs. 28a and 28b and a friction velocity of 0.29 m sec^{-1}, the values of $\sigma_u u_*^{-1}$ and $\sigma_v u_*^{-1}$ for Set I are respectively 4.56 and 4.88, being approximately twice the suggested values. The explanation of this may be attributed to Blackadar et al. (1974), who point out that the ratios depend on the mesoscale roughness which controls the low-frequency portion of the spectrum of the horizontal velocity components. Large-scale turbulent structure makes the largest contribution to the total variance over the recording period (provided the time scale of the turbulent fluctuations does not greatly exceed the sampling period), so that if variations bordering on the mesoscale are pronounced, the ratios can exceed 3. It already has been shown that large-scale systems of an oscillatory nature were present during the period of acquisition of data for this study.

The variation with height of the variance of vertical velocity, σ_w^2, over the 1-hr period for Set I is shown in Fig. 30. The values of σ_w^2 calculated for the three levels at which vertical

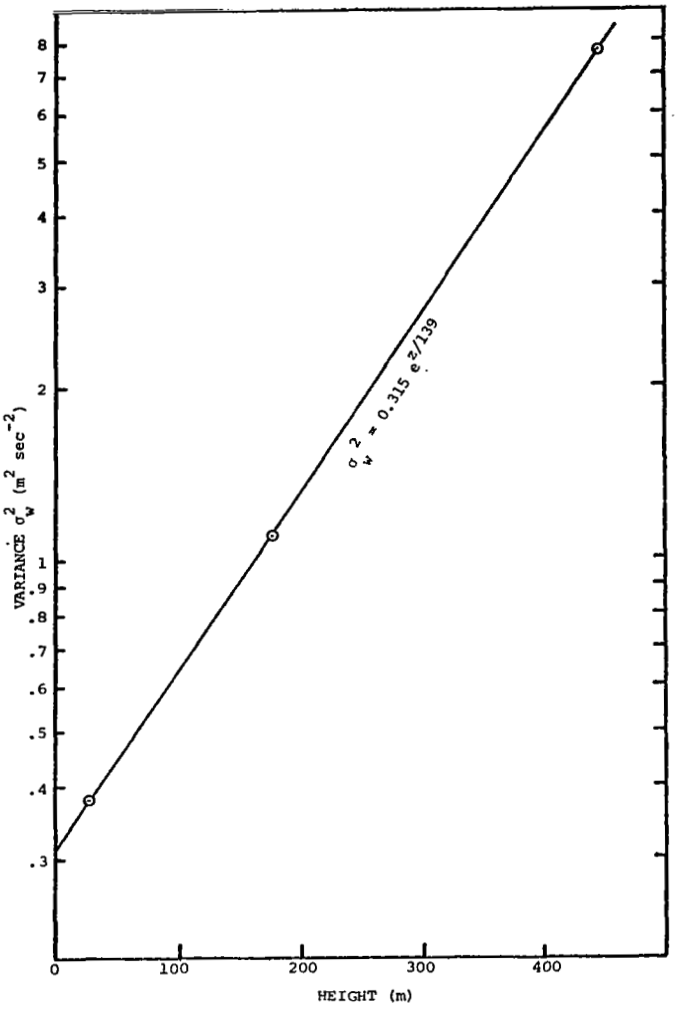

Fig. 30. Vertical component of variance as a function of height for the 1-hr period for Data Set I.

velocity was measured can be fit extremely well on the semi-logarithmic scale by the curve

$$\sigma_w^2 = 0.315e^{z/139} \quad , \tag{28}$$

in which z is the height in m. Equation (28) may be made non-dimensional by dividing each side by u_*^2:

$$\frac{\sigma_w^2}{u_*^2} = 3.75e^{z/139} \quad , \tag{29}$$

in which the units are the same as in (28).

The well-defined increase of σ_w^2 with height is due to the constraint the surface places on the vertical size of eddies, in that the proximity to the surface prevents the formation of low-frequency harmonics (Lumley and Panofsky, 1964). This rapid increase with height of σ_w^2 is indicative of the development of convection at the site, as evidenced by Fig. 31, which shows profiles for sequential 30-min periods for Set III. Referral to Fig. 7 shows that organized convective activity appeared only in about the last hour of the data set, and Fig. 31 shows an increase in σ_w^2 through the entire tower height only for the last two 30-min periods.

Near the surface the ratio, $\sigma_w u_*^{-1}$, from Data Set I of this study is 2.12 as compared to published values ranging from 0.7 to 1.33 (Lumley and Panofsky, 1964). The study by Pennell and LeMone (1974) gave a value of around 1.5 for $\sigma_w u_*^{-1}$ in the lower 400 m. Values of the ratio from the sequential 1-hr periods of Set II are shown in Table V, and are within the range of published values. Again, large-scale oscillations apparently cause the ratio from Set I to be slightly larger than that reported by other researchers.

The results presented in Figs. 28-32 are in good agreement with the theoretical results predicted by the numerical boundary layer model of Deardorff (1972) for the unstable case. Both the decrease of σ_u^2 and the rapid increase of σ_w^2 with height in the lower levels agree with the model. A predicted decrease

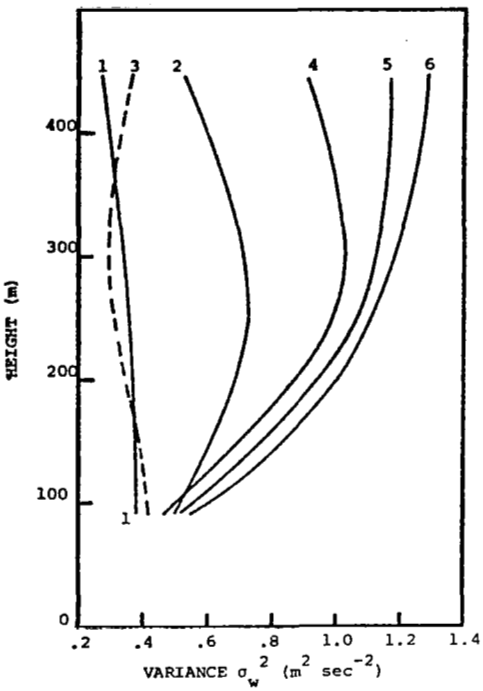

Fig. 31. Vertical component of variance as a function of height for sequential 30-min periods for Data Set III. Profile numbers refer to sequential 30-min averaging periods.

with height of σ_v^2 is not obvious in the results of this study; however, the lateral and longitudinal intensities should be nearly equal at all levels for the unstable case, a situation that does appear in the figures.

G. Turbulence Spectra

Power spectra were calculated by using the method of Blackman and Tukey (1958) and "hanning" smoothing for Data Set I for both hour and successive 15-min periods. A 15-min period contains 450 observations; the number of lags was chosen to be one-third the number of data points, or 150 lags. Thus, the frequency range was from 1 to 150 cycles(10 min)$^{-1}$ and the periods of oscillations capable of being examined ranged from 10 min down to 4 sec. The graphical result of plotting the smoothed spectrum, S(n), versus frequency, n, emphasizes the low-frequency harmonics but, unfortunately, is not area-conserving.

Normalized (area under the curve = 1) values of S(n) for Data Set I plotted against n calculated over the 1-hr period for the 26-, 177-, and 444-m levels are shown in Fig. 32. The slopes of these spectra may be compared to the -5/3 slope line also shown in the figure to determine to what extent, if any, the spectra follow the -5/3 power law characteristic of the inertial subrange. The low-frequency limit of the inertial subrange in the atmosphere is given (Lumley and Panofsky, 1964) by the Dougherty limiting wavelength, λ:

$$\lambda = L' \, Ri^{\frac{1}{4}} \quad , \tag{30}$$

where L' is the modified Monin-Obukhov length defined by (24) and Ri is the Richardson number. The Richardson number may be determined from the equation,

$$Ri = - \frac{gH}{C_p \bar{\rho} T} \left(u_*^2 \frac{\partial \bar{V}}{\partial z} \right)^{-1} \quad , \tag{31}$$

in which $\partial \bar{V}/\partial z$ is the vertical shear of the horizontal wind speed and the other variables are as in (24). Because the 1-hr mean wind profile is so nearly logarithmic with height (see Fig. 21), $\partial \bar{V}/\partial z$ may be approximated by differentiating (7) with respect to height, thereby yielding the expression for the shear:

$$\frac{\partial \bar{V}}{\partial z} = \frac{u_*}{kz} \quad , \tag{32}$$

where the variables are as before. Table VI shows the results of solving for the Dougherty limiting wavelength at the 26-, 177-, and 444-m levels and using 1-hr mean values for the appropriate variables in (24), (31), and (32). The low-frequency limit (cut-off frequency, n_λ) associated with λ at a level can be approximated by dividing the 1-hr, mean, horizontal, wind speed, $\bar{V}$, at that height by λ. The values of n_λ from Table VI can be compared with the frequencies in Fig. 32 at which the general slopes of the power spectra begin to deviate from the -5/3 slope. It is

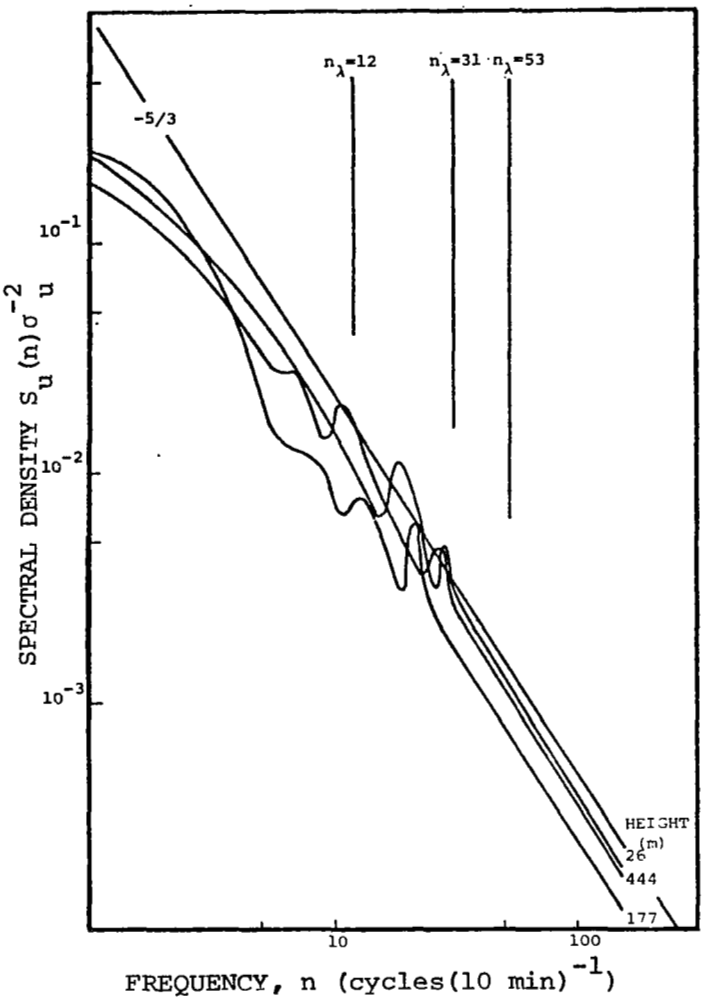

Fig. 32. Normalized spectra of longitudinal velocity for the 1-hr period at three levels for Data Set I. Slanted line labelled -5/3 indicates slope for inertial subrange. See text for explanation of cut-off frequencies, n_λ.

evident from the curves that the departure first takes place between 30 and 10 cycles/10 min. There is some indication from the 177- and 444-m level spectra of a progression of n_λ to higher frequencies with increasing height as predicted by (30). Lack of exact coincidence between the observed and predicted cut-off frequencies can be attributed to the assumption concerning the equality of the exchange coefficients, the approximation of the shear by (32), or the crudity in the use of $\bar{V}$ to obtain n_λ from λ. The important fact is that the observed power spectra apparently possess an inertial subrange in the high-frequency end extending to low frequencies in the vicinity of those at which the cut-off was predicted to occur.

Spectra of lateral velocity for the 1-hr period for Set I are shown in Fig. 33 in which $nS_v(n)u_*^{-2}$ is plotted against the frequency n. The value of u_*^2 for this period is 841 cm^2 sec^{-2}.

The spectra obtained at the NSSL facility are similar in shape to those described by other researchers. A comparison of the spectrum of lateral velocity over the 1-hr period at the 26-m level with an example presented by Lumley and Panofsky (1964) is shown in Fig 34. The latter was observed at Brookhaven at a height of 91 m; originally the spectral estimates were shown normalized by the square of the wind speed at 11 m, so the spectrum was multiplied by an arbitrary constant to make it comparable to that obtained at the NSSL tower. The similarity between the two curves in Fig. 34 is strong, and is presumable due to both spectra being observed during the daytime. Lumley and Panofsky state that the spectrum of lateral velocity is affected more by changes in stability rather than height, particularly in neutral or unstable air. Increasing instability increases the low-frequency portion (that end occupied by eddies predominantly convective in nature) of the spectra but leaves the high-frequency (dominated by mechanically-produced turbulence) portion, sensitive to roughness and wind speed, relatively unaffected. Spectra of lateral velocity observed at night show most of the variance partitioned to the high-frequency oscillations.

TABLE VI

Dougherty limiting wavelength λ and associated cut-off frequency n_λ, at three levels for Data Set I

Height (m)	T(°K)	H ($erg\ cm^{-2}\ sec^{-1}$)	Ri	λ (m)	$\bar{v}$ ($m\ sec^{-1}$)	n $cy(10\ min)^{-1}$
26	306.2	3600	-0.04	262	5.24	12
177	304.4	18000	-1.5	129	6.66	31
444	301.7	44200	-9.5	82	7.29	53

The curves in Fig. 33, all calculated for the 1-hr period, generally support this concept, but with the following two observations:

(1) Near the ground the production of mechanical turbulence adds a considerable amound of variance to the high-frequency oscillations. Above a sufficiently high level (between 26 and 177 m in this case) the variance in the high-frequency portion of the spectra truly approaches a constant with height.

(2) There is an increase of variance in the low-frequency oscillations with height, but the actual height above the surface is not necessarily the cause of the increase. Rather, the increase in the low-frequency portion of the spectra is consistent with the increase with height of the vertical heat flux shown in Fig. 5.

Further support for the concept may be derived from Figs. 35 and 36 in which $nS_v(n)\ u_*^{-2}$ for the lateral velocity is plotted versus n for the four 15-min periods for Set I at heights of 26 and 444 m, respectively. In each figure the high-frequency portions are approximately the same over the four periods, but there is considerable difference among the four 15-min periods at each level in the low-frequency end. Referral to Fig. 17 indicates the first two 15-min periods to be dominated by only slightly positive or strongly negative vertical heat flux, with

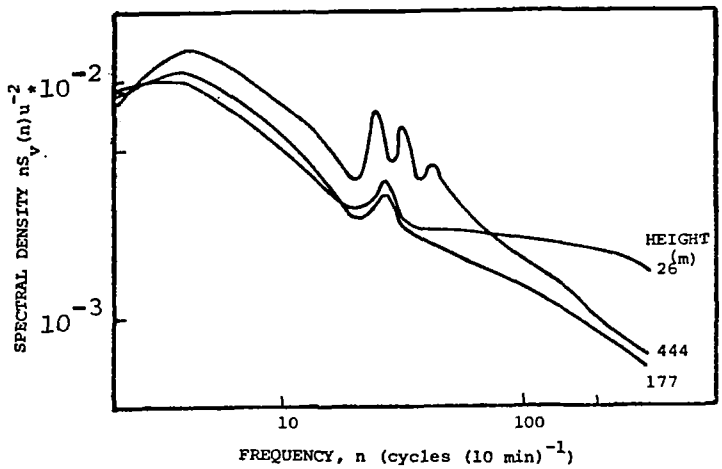

Fig. 33. Spectra of lateral velocity for the 1-hr period at three levels for Data Set I.

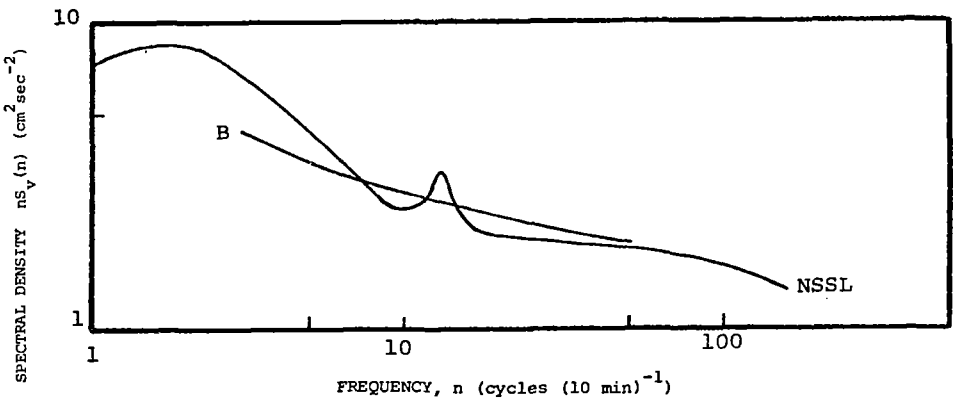

Fig. 34. Comparison of spectra of lateral velocity obtained from the NSSL and Brookhaven tower facilities. NSSL spectrum is for the 1-hr period at the 26-m level for Set I. Brookhaven spectrum (B) is for 91 m, taken from Lumley and Panofsky (1964).

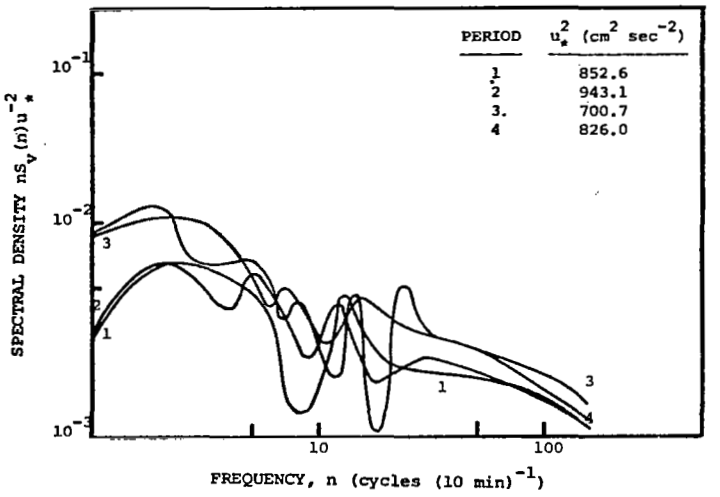

Fig. 35. Spectra of lateral velocity for sequential 15-min periods at the 26-m level for Data Set I.

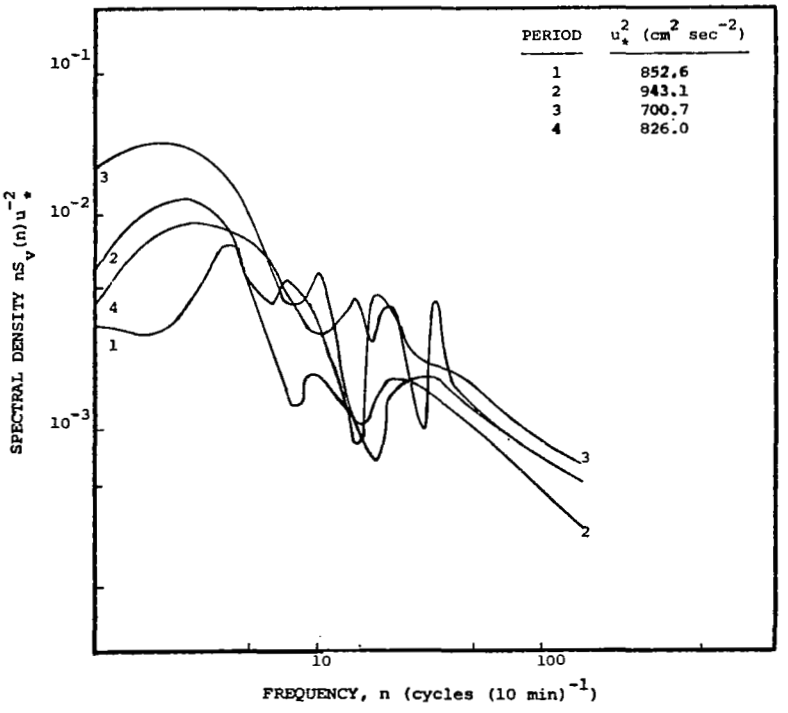

Fig. 36. Spectra of lateral velocity for sequential 15-min periods at the 177-m level for Data Set I.

the last two periods predominantly by positive vertical heat flux. The spectra for the first two 15-min periods at 26 m (Fig. 35) are below those for the third and fourth periods. Basically the same is true at the 177-m level (Fig. 36), viz., the fact that the curve pertaining to the fourth period is below that of the second probably is due to the return of strong negative heat flux at upper levels near the end of the fourth period.

Therefore, away from the strong influence of the surface, it appears that stability is the primary factor in determining the magnitude and shape of the spectrum of lateral velocity.

Spectra of longitudinal velocity for the 1-hr period at three levels (26, 177, and 444 m) for Set I are shown in Fig. 37, plotted in a manner similar to Fig. 34. Once again the influence of the ground is obvious in the increase of variance in the high-frequency portion of the spectrum at 26 m. The low-frequency portion, however, could not be dependent solely upon stability, as the spectrum of lateral velocity was, because there is considerable less variance partitioned at the 444-m level than at the 26-m level. Lumley and Panofsky (1964) report that the spectrum of longitudinal velocity is affected less by stability; thus, the relative difference between the spectra of the 444-m level and lower levels simply may reflect the decrease of mechanical turbulence (associated with wind shear) with height.

The effects of stability and the increase of height on the variance contained in a particular harmonic also are observable in the secondary peaks occurring between about 5 and 30 cycles $(10\ \text{min})^{-1}$ in Fig. 37. Particularly noticeable is the decrease in size of peak A from 26 to 444 m. The opposite is true of peaks C and D between the 177- and 444-m levels, where the increase with height may be related to the observed increase with height of the vertical heat flux.

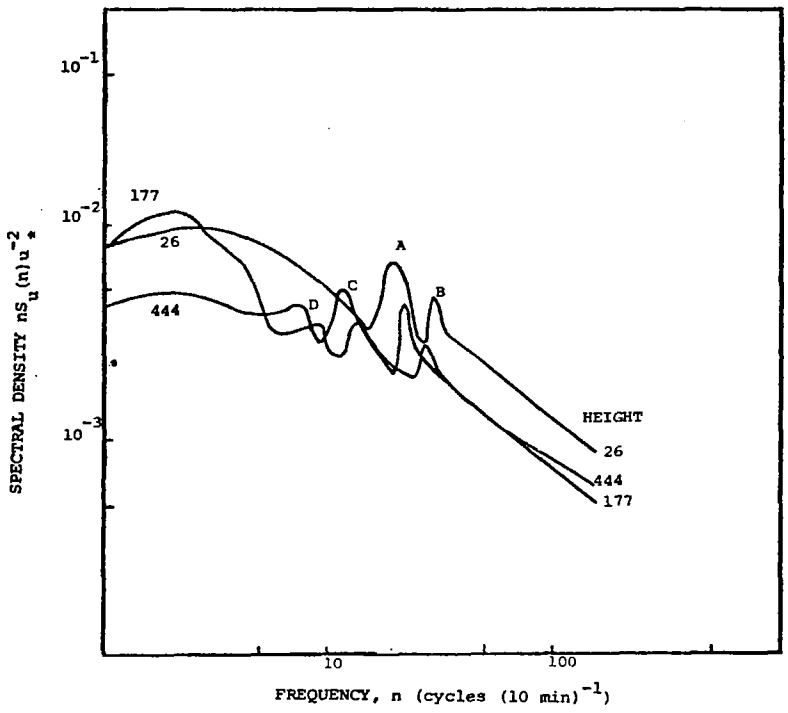

Fig. 37. Spectra of longitudinal velocity for the hour period at three heights for Data Set I.

Examination of the secondary peaks reveals another interesting feature -- the apparent shifting of peaks to higher or lower frequencies with increases in height. Peaks C and D are each apparently shifted by 2 cycles (10 min)$^{-1}$ between the 177- and 444-m levels. This conceivably could be due to energy being transferred to larger-scale eddies with height by accretion. Peak A appears to shift position from around 19 cycles (10 min)$^{-1}$ at 26 m to 21 cycles (10 min)$^{-1}$ at 177 m to 27 cycles (10 min)$^{-1}$ at 444 m.

Whereas the spectra of the horizontal velocity components are influenced only to a degree by height, spectra of vertical velocity are strongly dependent upon this variable. The scale of vertical velocities increases with height due to the limiting effect of the proximity of the surface on the energy contained

in low wave numbers. Lumley and Panofsky (1964) suggest that this scale is a linear function of height, and from similarity theory the spectrum may be predicted by

$$\frac{nS(n)}{u_*^2} = F\left(\frac{nz}{\bar{V}}, Ri\right) \quad , \tag{33}$$

where $nS(n)u_*^{-2}$ is the spectrum, Ri the Richardson number, $nz\bar{V}^{-1}$ the non-dimensional frequency (essentially the ratio of height to wavelength), and F a universal function. When $nS(n)u_*^{-2}$ is plotted against $nz\bar{V}^{-1}$ the proportionality of the scale to height is taken into account so that spectra should show no shift with height (on the assumption that the dependence upon Ri is negligible). The authors cited above have shown this to be the case up to a height of a few hundred meters, above which the scale approaches a constant and the maxima of the spectra exhibit a characteristic shift from around $nz\bar{V}^{-1} = 0.25$ to higher frequencies.

Spectra of vertical velocity obtained from the NSSL tower over the hour period at three levels (26, 177, and 444 m) for Set I are shown in Fig. 38, in which $nS_w(n)u_*^{-2}$ is plotted against the non-dimensionalized frequency $nz\bar{V}^{-1}$. The values of $\bar{V}$ are 1-hr mean wind speeds for the appropriate levels. If one ignores the superimposed peak at around f = 0.04 in the spectrum at the 26-m level, the curves at the 26- and 177-m levels are very similar in shape to those described by Lumley and Panofsky (1964) and Panofsky *et al.* (1967), with the spectral peaks occurring at around $nz\bar{V}^{-1} = 0.2$. Thus the linear function of scale to height is supported by the results presented in the figure. The increase exhibited by the high-frequency portion of the spectrum at 444-m is surprising and as yet unexplained. The curves in Fig. 39 that represent the spectra of lateral velocity from Fig. 33 plotted against $nz\bar{V}^{-1}$ demonstrate the shifting that occurs when the scale of turbulence is not a function of height.

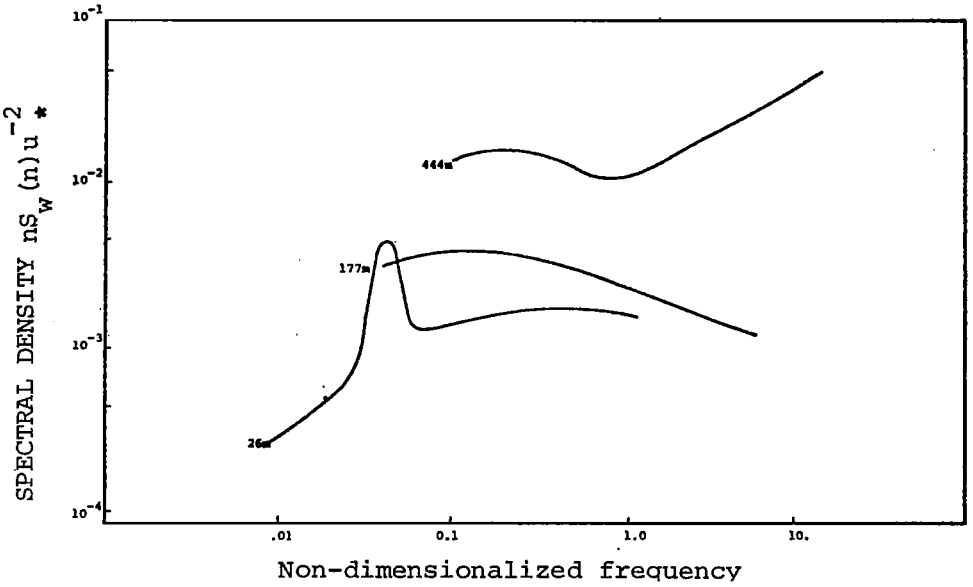

Fig. 38. Spectra of vertical velocity for the hour period at three levels as a function of non-dimensionalized frequency $nz/\overline{V}$ for Data Set I.

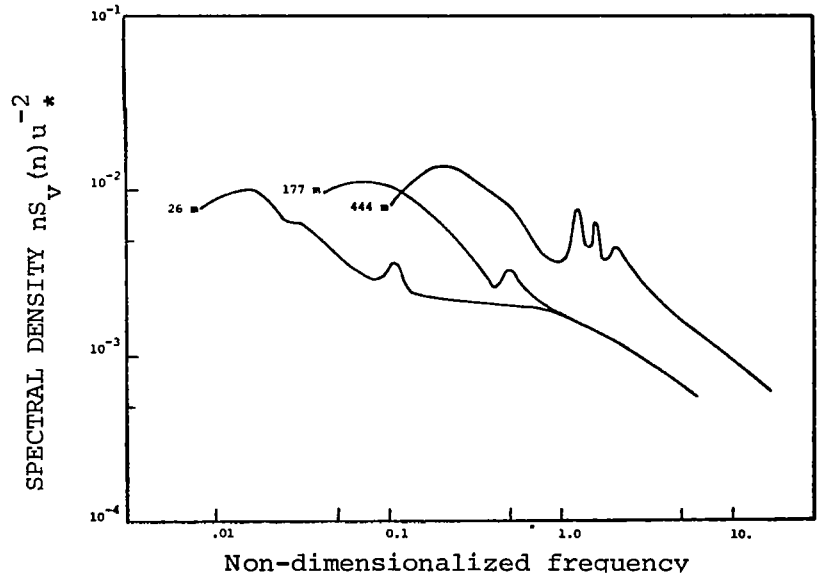

Fig. 39. Spectra of lateral velocity for the hour period at three levels as a function of non-dimensionalized frequency $nz/\overline{V}$ for Data Set I.

Similar results were obtained from the spectral analysis of the two other sets of data. Normalized spectra of the longitudinal component velocity at the 89-m level for Set III are shown in Figs. 40 and 41 for sequential periods of 30 min. The curves in the two figures are similar to corresponding spectra in Fig. 32, and possess a fairly large segment in the high-frequency end that conforms to the -5/3 slope. The spectra have been divided into two groups, with those having total variance greater than 0.5 m^2 sec^{-2} in Fig. 40, and those with less than 0.5 m^2 sec^{-2} in Fig. 41. For frequencies greater than around 1 cycles min^{-1}, the curves of the two figures are roughly the same. For lower frequencies, however, the spectra in Fig. 40 ($\sigma_u^2 > 0.5$ m^2 sec^{-2}) rise to a sharp peak at around 3 to 4 cycles $(10\ min)^{-1}$, while in Fig. 41 ($\sigma_u^2 < 0.5$ m^2 sec^{-2}) the spectra flatten off to a broad peak of the same order of magnitude as the secondary peak located at around 9 cycles $(10\ min)^{-1}$ in each curve. Apparently, the spectra containing more total energy (variance) hold this energy in the low-frequency peak.

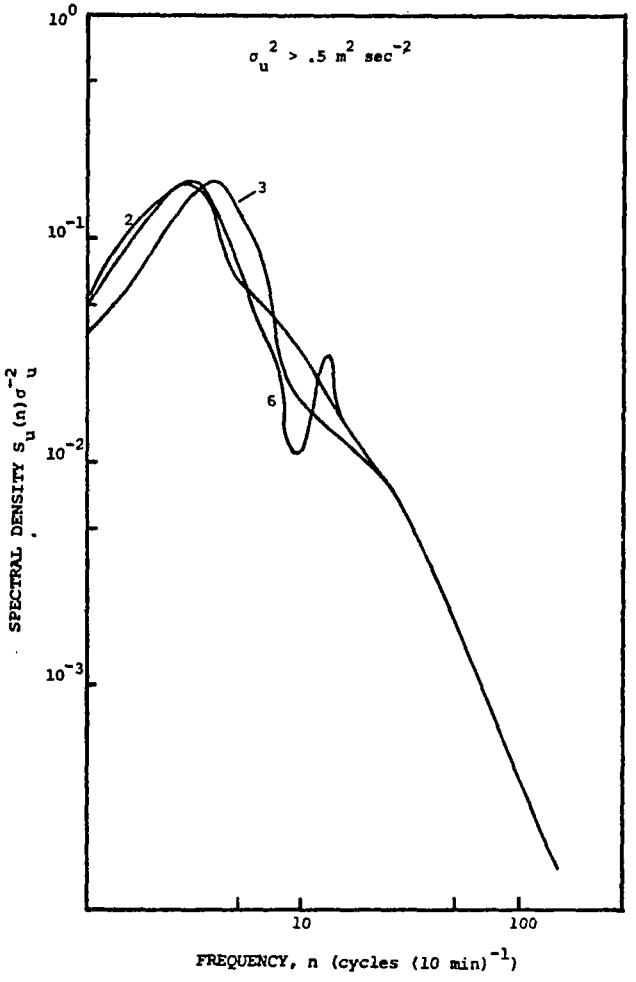

Fig. 40. Spectra of longitudinal velocity at the 89-m level for 30-min periods of Data Set III with total variance greater than 0.5 m^2 sec^{-2}.

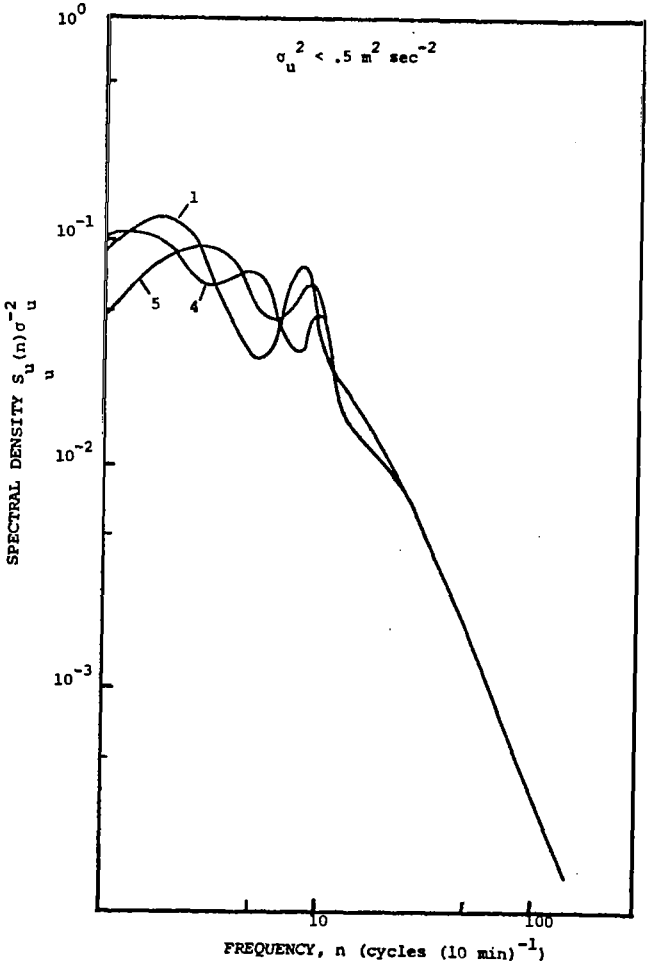

Fig. 41. Spectra of longitudinal velocity at the 89-m level for 30-min periods of Data Set III with total variance less than 0.5 m^2 sec^{-2}.

5. INTERRELATIONSHIPS OF THE PROPERTIES OF ATMOSPHERIC TURBULENCE BELOW A HEIGHT OF 500 METERS

The causes behind the behavior of any particular parameter of turbulence in the friction layer ultimately must depend upon the physical and geometrical nature of the turbulence occurring at the time of observation. Outside the laboratory, the determination of the actual structure generally is not possible, so that the structure must be inferred from the measured parameters. In the previous section, the profiles of shearing stress and vertical heat flux indicated the likely presence in the unstable friction layer of both mechanical and buoyant sources of turbulence coexisting in the layer below 500 m. Spectrum analysis has shown that the size of eddies increases with height and that the large-scale fluctuations are predominantly important in the turbulent transfer process. With these and other findings from Section 4 in mind, a simple model for this region of the friction layer can be outlined that describes the general behavior of some of the parameters of turbulence.

Some indication of the structure of turbulence in the unstable friction layer is given in Fig. 42, in which the difference between successive 5-min and 1-hr average values of wind speed at a level from Data Set I are plotted as a function of time (period number of the 5-min averages). The variation of this difference, which reflects the variation of the measured wind speed, is practically the same for all the four lowest levels (26, 45, 90, and 177 m). The similarity between the three highest levels (266, 355, and 444 m) also is obvious, with the magnitude of the 266-m level trace intermediate between that of the adjacent levels. Apparently there exists a level at around 200 m that marks a transition in the character of the friction layer, where fluctuations of wind speed above the transition are controlled in a manner dissimilar to that below the transition. It is unlikely that the transition occurs at a quasi-finite boundary but the zone is thin enough to exist between the 177- and 266-m levels in several instances, a thickness of less than 100 m.

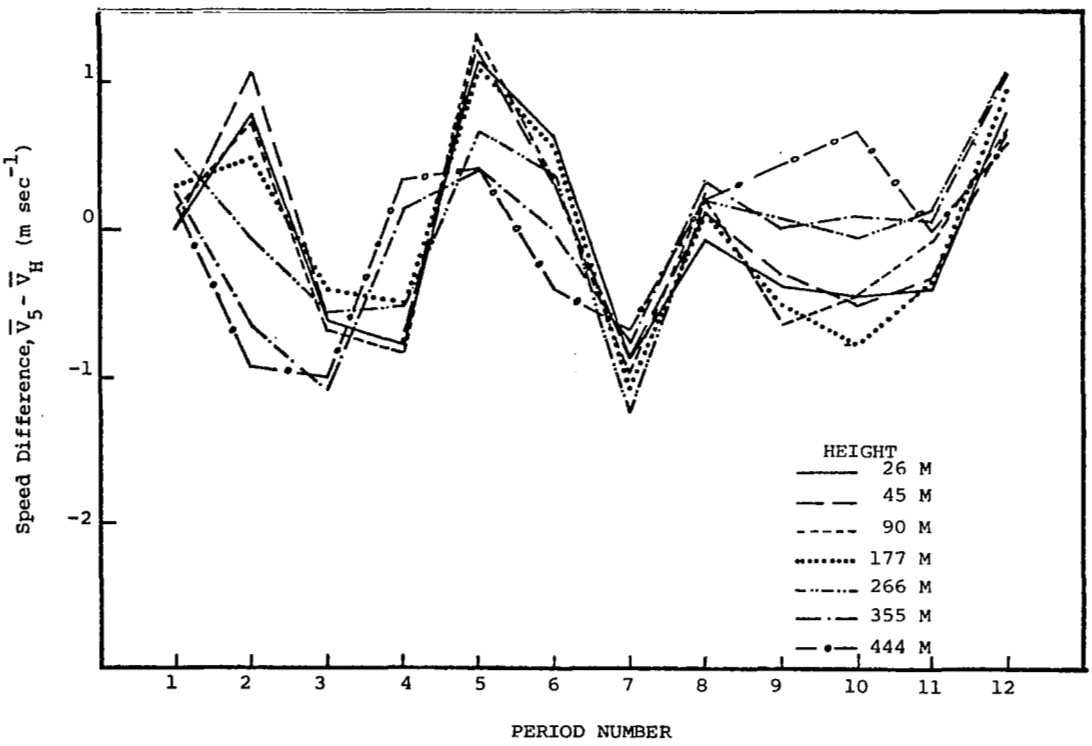

Fig. 42. Variation of 5-min mean wind speed $\overline{V}_5$ at seven levels around its respective 1-hr mean value, $\overline{V}_H$, for Data Set I.

The variation with height of the standard deviation of vertical motion, σ_w, is useful in determining the possible controlling factors in the upper and lower regions. Values of σ_w obtained from (28) are shown in Fig. 43 plotted against height. Although the increase with height of this variable is due to the limiting effect of the proximity to the ground on oscillations in the vertical, the shape of the curve is determined by the type of turbulent activity present through the layer. The curve obtained from the solution of (28) may be compared with theoretical profiles corresponding to purely forced (mechanical) and free (buoyant) convection, also shown in Fig. 43. Lumley and Panofsky (1964) show that the change of σ_w with height for forced convection is given by the equation,

$$\sigma_w = A(u_*^3 \frac{\partial \overline{V}}{\partial z} z)^{1/3} , \qquad (34)$$

in which A is a constant and the remaining symbols are as in previous equations. For free convection, these authors give the equation,

$$\sigma_w = B\left(\frac{gHz}{C_p\bar{\rho}T}\right)^{1/3} , \qquad (35)$$

where B is a constant and the other symbols are as before. When (34) and (35) are solved by using 1-hr mean values for the dependent variables, the theoretical profiles are as in Fig. 43. Because the 1-hr mean wind profile for Set I approximates the log-law profile very closely, (32) was used to calculate the wind shear in (34). In addition, the theoretical σ_w profiles were forced to coincide with the observed profile at the 26-m level by the choice of appropriate values for the constants A and B, which turned out to be 1.55 and 4.49, respectively. The fact that the value of σ_w is constant with height for forced convection is a direct result of the wind profile being logarithmic.

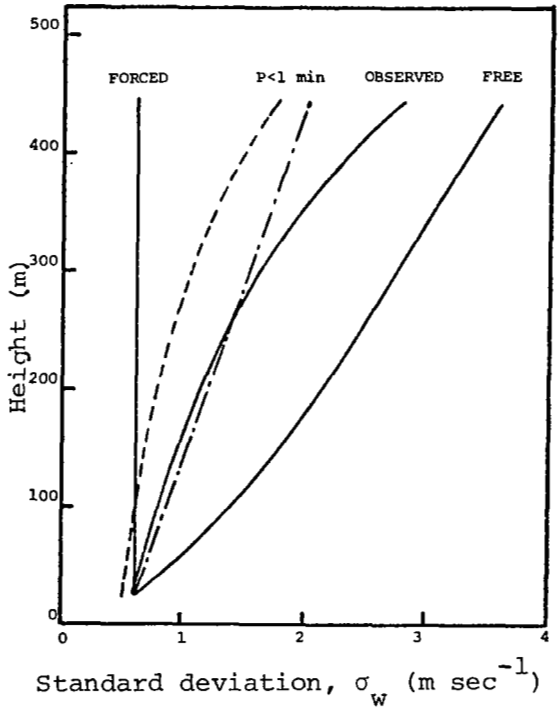

Fig. 43. Observed and theoretical profiles of the standard deviation of vertical velocity for Data Set I. Dashed line shows the effect of excluding harmonics with periods greater than 1 min. Dash-dot line is the solution of equation (38) in text.

The observed profile of σ_w lies between the theoretical profiles for forced and free convection, as might be expected.

Observed values of the standard deviation approach the theoretical curve associated with forced convection at the lower levels, while at the higher levels the observed σ_w curve approximates the profile due to free convection.

The variation with height of the production of turbulent kinetic energy (KE) for Set I is shown in Fig. 44. Mechanical production of KE is proportional to the vertical shear of the horizontal wind and may be obtained from the equation (Campbell et al., 1970):

$$\varepsilon_m = u_*^2 \frac{\partial \bar{V}}{\partial z} , \tag{36}$$

where ε_m is the production rate of KE per unit mass due to mechanical processes, and the remaining symbols are as before. Again, $\partial\bar{V}(\partial z)^{-1}$ was calculated by using (32). These authors give for the buoyant production of KE the equation,

$$\varepsilon_h = \frac{gH}{C_p \bar{\rho} T} , \tag{37}$$

where ε_h is the production rate per unit mass of KE by buoyancy processes, and the other symbols are as before. The curves in Fig. 44 were determined by solving (36) and (37) with the use of 1-hr mean values of the dependent variables.

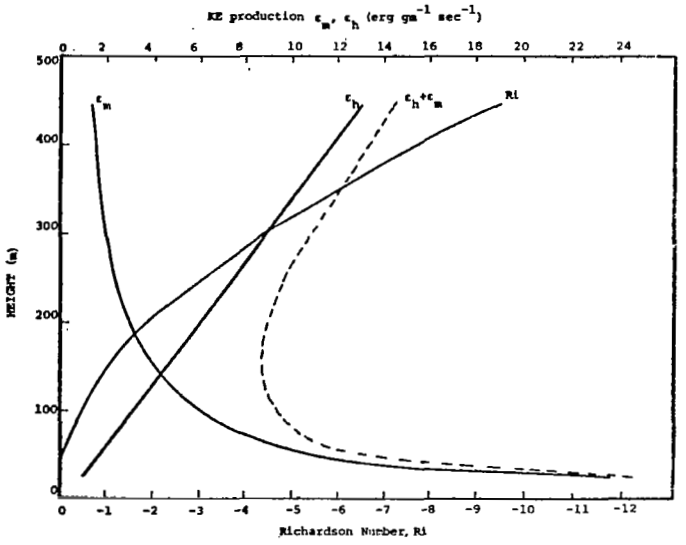

Fig. 44. Variation of turbulent kinetic-energy (KE) production and Richardson number with height for Data Set I.

The curve labeled $\varepsilon_m + \varepsilon_h$ represents the combined KE production by both mechanical and buoyant means. The dominance of ε_m over ε_h near the surface is due to the large wind shear near the surface and explains why the wind profile can be logarithmic near the ground even in unstable conditions. At the upper levels where wind shear is negligible, the increase of H with height (see Fig. 15) causes ε_h to dominate ε_m.

From calculated values of the production of turbulent kinetic energy, an estimate of the variation with height of σ_w may be obtained from the relation (Lumley and Panofsky, 1964),

$$\sigma_w = c\ [z(\varepsilon_m + \delta\varepsilon_h)]^{1/3}\ , \tag{38}$$

where c is a constant and δ is a coefficient that relates the relative efficiency with which wind shear and convection produce turbulence (generally assumed to be $\sim$4). With values from Figs. 43 and 44 for σ_w, ε_m, and ε_h, (38) may be solved at the 26-m level for c. In this case the value of the constant turns out to be around 1.5. Values of σ_w obtained from (38) are shown in Fig. 43 as a function of height, and the observed and calculated values agree rather well, when one considers the assumptions used in solving (38). It is not unlikely that δ could be a function of height, thereby allowing an even better agreement between observed and theoretical values of σ_w.

The profile of ε_m in Fig. 44 is identical to profiles of the mechanical production of turbulent KE appearing in a recent report by Lenschow (1974). Profiles of ε_h appearing in that report show a linear decrease with height, but the observations were made in November in relatively cold air passing over the Great Lakes, so the conditions do not allow values of ε_h to be compared.

Also shown in Fig. 44 is the variation with height of the Richardson number, Ri, for Set I defined by the equation (Lumley and Panofsky, 1964),

$$Ri = -\frac{\left(\frac{gH}{C_p\bar{\rho}T}\right)}{u_*^2\left(\frac{\partial\bar{V}}{\partial z}\right)} = -\frac{\varepsilon_h}{\varepsilon_m}\ , \tag{39}$$

in which the symbols are the same as in previous equations. In (39) the ratio of the exchange coefficients of heat and momentum is assumed to be 1. The rapid decrease in Ri from approximately -0.004 (near-neutral) at 26 m is indicative of the rapid decrease with height of the magnitude of ε_m.

The production of turbulent KE by buoyancy processes dominates that by mechanical means from around 200 m to the top of the tower. The curve representing combined KE production exhibits a minimum just below the 200-m level, and above the 200-m level the profile of Ri shows the air becoming rapidly more unstable with height. Therefore, in the region above the transition, the characteristics of turbulent activity are determined by convection, while in the lower region they are functions primarily of wind speed and surface roughness. The sequential, 15-min, average, wind-speed profiles shown in Fig. 21 support this proposition. Regardless of the vertical-motion or heat-flux conditions (see Figs. 4 and 15) for a particular 15-min period, the portion of the wind speed profile below about 200 m is very closely logarithmic. Above the 200-m level, systematic deviations of up to 1 m sec^{-1} from the log-law profile are evident and, as pointed out earlier, are correlated with to the general fields of vertical motion and heat flux. In addition to the variation with height of observed σ_w, Fig. 43 also displays the increase with height of the standard deviation of vertical velocity contained in oscillations with periods less than 1 min, which excludes a fair portion of the harmonics due to convection. Whereas the excluded portion amounts to only around 17 per cent of the total observed σ_w at 26 m, it accounts for approximately 38 per cent at 444 m. Thus, the nature of the parameters of turbulence appears to be determined by convection at the upper levels of the region penetrated by the NSSL tower and by wind speed and surface roughness at the lower levels.

Lumley and Panofsky (1964) and Munn (1966) have proposed a model of the friction layer under unstable conditions that is similar to that suggested in the previous paragraph, except in

their choice of the level at which the transition from predominantly forced to free convection takes place. However, the exact level where this takes place is certainly a function of the relative magnitudes of stability, wind speed, and roughness, so the qualitative agreement of the two models still is good. Briefly, these authors proposed that, in the layer adjacent to the ground, the shear production term, ε_m, dominates the buoyancy term, ε_h, under all stability conditions, so that the turbulent structure is similar to that found under neutral conditions. The layer above this surface layer contains rather large-scale vertical motions, well correlated with temperature, so that energy is exported from this region upward. It is suggested that this "thermal turbulence" does not interact to a great degree with the "mechanical turbulence" at these levels, and the latter must be relatively small due to the small magnitude of shear at these heights.

Results of the analysis of the two other data sets indicate that, for periods on the order of 30 min or longer, the average wind-speed profile approaches a logarithmic shape as the friction layer becomes more unstable and convection becomes more organized. The mean wind values from Set II (see Fig. 23) tended to approach log-law values at successively higher levels for later periods, as the layer penetrated by the tower progressed from a temperature inversion situation to unstable conditions.

6. SUMMARY OF RESULTS

This investigation of the detailed structure of turbulence in the friction layer below a height of 500 m utilized shearing stresses, vertical heat fluxes, and spectral statistics calculated from covariances and turbulent fluctuations determined from the fluid motion. Results were drawn from the analysis of several hours of detailed observations under unstable and stable-becoming-unstable conditions. Specific conclusions reached through this investigation include:

1) In the unstable friction layer below 500 m, the variation with height of wind speed averaged over periods of the order of 15 min or longer tended to approach the logarithmic profile,

$$\overline{V} = \frac{u_*}{k} \ln\left(\frac{z}{z_o}\right) ,$$

throughout the tower height. In cases where convection is still poorly organized, the log-linear law,

$$\overline{V} = \frac{u_*}{k}\left(\ln\left(\frac{z}{z_o}\right) + \beta\frac{z}{L}\right) ,$$

was useful in determining the wind speed relative to the log-law value at a level.

2) For the layer below 500 m, the vertical heat flux and standard deviation of vertical motion may be approximated by the equations,

$$H = \overline{\rho} C_p \frac{\partial T}{\partial t} z + H_o$$

and

$$\sigma_w = c\left[z\left(\varepsilon_m + \delta\varepsilon_h\right)\right]^{1/3}$$

respectively.

3) For the unstable friction layer below 500 m, profiles of vector shearing stress, vertical heat flux, and variance of vertical motion may be fit by the empirical relations,

$$\left|\vec{\tau}\right|/\tau_o = 2.1 \ln\left(\frac{z}{7.3}\right) ,$$

$$\frac{H}{\overline{\rho} C_p T_o^* u_*} = 3.88z + 0.4 ,$$

and

$$\frac{\sigma_w^2}{u_*^2} = 3.75e^{z/139} ,$$

respectively.

4) The power spectrum of lateral velocity is dependent primarily upon stability above the influence of the surface, while the spectrum of longitudinal velocity is dependent upon both stability and surface roughness. The scale of vertical oscillations appears to increase linearly with height.

5) In the spectrum of longitudinal velocity, the inertial-like subrange extends from the high-frequency end into the range from 30 to 10 cycles(10 min)$^{-1}$.

6) A zone of transition exists in the friction layer near 200 m. Turbulent activity in the lower region is controlled by wind speed and surface roughness, while in the upper region convective activity dictates the character of turbulence.

7) The approach of the observed mean wind profile to the logarithmic profile follows the increase in convective activity as the day progresses from early morning to early afternoon.

REFERENCES

Blackadar, A. K., and H. A. Panofsky, 1969: "Wind profiles, spectra, and cross-spectra over homogeneous terrain," ECOM-01388-3, 71 pp.

Blackadar, A. K., H. A. Panofsky, and Franz Fiedler, 1974: "Investigation of the turbulent wind field below 500 feet altitude at the Eastern Test Range, Florida," NASA CR-2438, 86 pp.

Blackman, R. B., and J. W. Tukey, 1958: The Measurement of Power Spectra, New York, Dover Publications, 190 pp.

Bradham, John H., 1970: "An analysis of the variation of the shearing stresses and momentum exchange in the friction layer over Cape Kennedy, Florida," M.S. Thesis, Texas A&M University, 50 pp.

Campbell, Gaylord S., Frank V. Hansen, and Raymond A. Dise, 1970: "Turbulence data derived from measurements on the 32-meter tower facility: White Sands Missile Range, New Mexico," ECOM-5314, 72 pp.

Carl, D. M., T. C. Tarbell, and H. A. Panofsky, 1973: "Profiles of wind and temperature from towers over homogeneous terrain," J. Atmos. Sci., 30(5):788-794.

Carter, John K., 1970: "The Meteorologically Instrumented WKY-TV Tower Facility," ERLTM-NSSL 50, 18 pp.

Charnock, H., J. R. D. Francis, and P. A. Sheppard, 1956: "An investigation of wind structure in the trades," Phil. Trans. Roy. Soc., London, 249(963):179-234.

Deardorff, James W., 1972: "Numerical investigation of neutral and unstable planetary boundary layers," J. Atmos. Sci., 29(1):91-115.

Kjelaas, A. G., D. W. Beran, W. H. Hooke, and B. R. Bean, 1974: "Waves observed in the planetary boundary layer using an array of acoustic sounders," J. Atmos. Sci., 31(8):2040-2045.

Lenschow, D. H., 1974: "Model of the height variation of the turbulence kinetic energy budget in the unstable planetary boundary layer," J. Atmos. Sci., 31(2):465-474.

Lettau, Heinz, 1950: "A re-examination of the 'Leipzig Wind Profile' considering some relations between wind and turbulence in the frictional layer," Tellus, 2(1):125-129.

Lumley, J. L., and H. A. Panofsky, 1964: The Structure of Atmospheric Turbulence, New York, John Wiley and Sons, 239 pp.

Munn, R. E., 1966: Descriptive Micrometeorology, New York, Academic Press, 245 pp.

Panofsky, H. A., N. Busch, B. Prasad, S. Hanna, E. Peterson, and E. Mares, 1967: "Properties of wind and temperature at Round Hill, South Dartmouth, Mass.," ECOM-0035-F, 93 pp.

Pasquill, F., 1950: "The aerodynamic drag of grassland," Proc. Roy. Soc., London, 202(1068):143-153.

Pena, Ricardo, Laurence J. Rider, and Manuel Armendariz, 1972: "Turbulence characteristics at heights of 1.5, 4.0 and 16.0 meters at White Sands Missile Range, New Mexico," ECOM-5421, 38 pp.

Pennell, W. T., and M. A. Lemone, 1974: "An experimental study of turbulence structure in the fair-weather trade wind boundary layer," J. Atmos. Sci., 31(5):1309-1323.

Powell, David C., and C. E. Elderkin, 1974: "An investigation of the application of Taylor's Hypothesis to atmospheric boundary layer turbulence," J. Atmos. Sci., 31(4):990-1002.

Scoggins, James R., 1966: "Ground wind measurements and anemometer response," Paper presented at the Meeting on Ground Wind Load Problems in Relation to Launch Vehicles, NASA-Langley Research Center, Langley Station, Hampton, Virginia.

Scorer, R. S., and F. H. Ludlam, 1953: "Bubble theory of penetrative convection," Quart. J. Roy. Meteor. Soc., 79:94-104.

Sutton, O. G., 1953: Micrometeorology, New York, McGraw-Hill Book Co., Inc., 333 pp.

Tennekes, H., 1973: "The logarithmic wind profile," J. Atmos Sci., 30(2):234-238.

Thuillier, R. H., and V. O. Lappe, 1964: "Wind and temperature profile characteristics from observations on a 1400 ft tower," J. Appl. Meteor., 3:299-306.